Potsdam Institute for Climate Impact Research

Indigenous Lands Moisture Tracking Project

Lauren Andersen, Caterina Vanelli, Simon Fahrländer

December 2025

unesco Centre Under the auspices of UNESCO

International Centre for Water Cooperation

HOSTED BY SIWI

ISBN: 978-91-88495-27-3

How to cite
Andersen, L., Fahrländer, S., Vanelli, C., 2026. Indigenous Lands Moisture Tracking Project. Potsdam Institute for Climate Impact Research, International Centre for Water Cooperation, and Stockholm International Water Institute.

Cover photo
Reindeers in Yllas Pallastunturi National Park, Lapland, Finland. Alberto Gonzales, Shutterstock.

Authors
Lauren Andersen, Simon Fahrländer, Caterina Vanelli. Potsdam Institute for Climate Impact Research

Editing, layout, and publishing
SIWI

Contact
Stockholm International Water Institute
Kabyssgatan 4D, 120 30 Stockholm, Sweden
Visiting Address: Hammarbybacken 31
www.siwi.org

Contents

Preface

This report presents key findings from the project “Indigenous Territories Contribution to Atmospheric Moisture Flows”, commissioned by the International Centre for Water Cooperation (ICWC), a UNESCO Category II Centre hosted by SIWI. The study was carried out by the Potsdam Institute for Climate Impact Research (PIK) in close collaboration with SIWI, with the analytical approach and parameters developed jointly through expert discussions between the two organizations.

The main aim of the project was to quantify the contribution of indigenous peoples' lands (IPL) to local, regional, and global scale moisture flows and terrestrial moisture recycling (TMR), building on three objectives. First, to quantify how much water originating from IPL contributes to global atmospheric moisture flows, in particular terrestrial rainfall through TMR. Second, to better understand and assess the value of water that comes from land under Indigenous stewardship. Third, to inform international policy so that the role of Indigenous Peoples and their territories in sustaining global hydrological cycles is better recognised and reflected in climate and water policy and governance.

1. Project Background

Precipitation[1] is globally sourced from atmospheric moisture (or water vapour), which itself is sourced from evaporation from the ocean surface and evapotranspiration (ET) from land-based sources, the latter of which includes evaporation from bare soil, evaporation from the surface of terrestrial water bodies (wetlands, lakes, reservoirs, rivers, streams, etc.), evaporation of water intercepted by plants and transpiration[2] from vegetation (forests, grasses, crops, etc.). The flow of water from land to the atmosphere is often referred to as **green water flow**, as it describes the flux of plant available water, termed green water, which includes all forms of terrestrial ET described above (e.g. Falkenmark & Rockström, 1996). Once in the atmosphere, this moisture is subsequently transported, termed **atmospheric moisture flow**, according to local wind patterns, large scale convection patterns and pressure gradients, among other factors. The global hydrological cycle is therefore characterised by a continuous exchange of moisture between the ocean and land, with the trajectories of atmospheric moisture flows from source to sink potentially spanning continents and oceans.

Terrestrial moisture recycling (TMR) describes the process by which moisture which originates anywhere on land contributes to precipitation anywhere on land (e.g. van der Ent et al., 2010). In other words, when green water flow precipitates back on land. Case studies of moisture recycling often investigate instances where the moisture source and sink are considered the "same" given the research interest- this could describe a certain location, e.g. moisture recycling within or between basins, regions, countries or continents, or a particular quality (regardless of spatial proximity), e.g. moisture recycling within or between forests, agricultural lands, protected areas, biomes or indigenous territories. Local to global scales are relevant, ranging from the tight feedback loops of local recycling to the trans-oceanic transport of moisture from one continent to another.

Compared to oceanic evaporation coming from a relatively plentiful and stable moisture source, terrestrial ET is vulnerable to land cover and land use changes. Any action or outcome in a source area that impacts green water flow, e.g. deforestation, agricultural practices, loss of soil moisture, will not only have local consequences, but impacts to the precipitation potential in downwind sink areas. Therefore, ecosystems intact in their functioning and managed lands which minimise adverse impacts on hydrological functioning are critical to preserving green water flows and their subsequent TMR.

The International Centre for Water Cooperation (ICWC), hosted by Stockholm International Water Institute (SIWI) is interested in furthering our understanding of what types of governance, management and stewardship are achieving these goals, especially in relation to Indigenous Peoples, who have unique knowledge and long-standing ties to their ancestral lands and waters. However, many modern governance and conservation approaches have overlooked their essential role, knowledge and land rights (Fletcher et al., 2021). At least a quarter of the world's terrestrial

[1] Precipitation is water from the atmosphere that falls to the ocean or land surface. The term precipitation includes water in any liquid or solid form – rain, snow, hail, etc. – which is why the term rainfall is commonly used in regions that don't receive ample snowfall.

[2] Through the process of photosynthesis, plants uptake soil water via their roots, then transpire water as vapour through their open stomata as CO_2 enters.

lands are under indigenous stewardship, and these lands encompass about 40% of all terrestrial protected areas and ecologically intact landscapes (Garnett et al., 2018), including 36.2% of the world's intact forest lands (Fa et al., 2020). It is estimated that 45% of terrestrial precipitation is sourced from terrestrial green water flow (De Petrillo et al., 2025), meaning it is TMR, but there is little understanding of the extent and role that indigenous territories play in global hydrological flows, including TMR.

This project aims to quantify the contribution of Indigenous Peoples' lands (IPL) to regional and global scale TMR. This represents a quantitative first step in revealing the extent to which indigenous stewardship of these lands provides global and regional ecosystem services. To answer this question in its most basic form requires first mapping or acquiring an appropriate dataset of Indigenous Peoples' lands globally, harmonised such that the level of detail is comparable across regions. With an understanding of where IPL are globally, a quantitative accounting of the fate of IPL green water flow can be performed to understand how much terrestrial precipitation is sourced from IPL. From here, comparisons with non-IPL lands and analysis of regional and seasonal dynamics are possible.

2. Mapping Indigenous Peoples' Lands

2.1 The Garnett et al. (2018) dataset

Published in *Nature Sustainability* in 2018, the mapping effort by Garnett et al., (2018) is the first globally aggregated dataset of IPL, and to our knowledge, remains the most comprehensive globally harmonised map of IPL. The Garnett et al., (2018) global map of terrestrial lands managed or owned by Indigenous Peoples is based on publicly available geospatial resources (127 data sources in total), including cadastral records for state-recognised IPL, publicly accessible participatory mapping, models based on census data and maps derived from scholarly publications. Their definition of IPL encompasses not only areas where Indigenous Peoples' land tenure is officially recognised, but also areas where Indigenous Peoples maintain a substantial influence over land management. Through this process and given this definition, they identified that Indigenous Peoples' lands cover at least ~38 million km^2 on all inhabited continents and in 87 countries or administratively independent entities (out of 235, excluding Antarctica and uninhabited islands in the Southern Ocean). Areas with no mapped IPL do not necessarily indicate or confirm an absence of Indigenous Peoples or their lands, but rather areas for which an indigenous connection cannot be inferred based on the publicly available geospatial data sources used.

The Garnett et al., (2018) dataset is widely used in global IPL studies, making it advantageous to use for this study, as it ensures comparability with other publications (Fa et al., 2020;Owen et al., 2022; Sze et al., 2022). We received the data after signing an ethics declaration, which, among others, requests that the IPL data does not become publicly available to prevent intentional and unintentional harm to Indigenous Peoples. The data includes the original shapefiles, classified by country, and a gridded product at 100 km^2 scale.

Each grid is assigned a value according to how much IPL are present in each grid, ranging from 0 – 1, where a grid with no IPL = 0, a grid with 50% IPL = 0.5 and a grid with 100% IPL = 1. At the sub-grid scale, the precise location of the IPL are not known, only the proportion of IPL within that grid. As this IPL map is the basis of our subsequent moisture tracking study, further post-processing was necessary for alignment with the grid scale that our moisture flow model operates. We therefore re-gridded the original map to a 0.5-degree grid which is 55.5 km^2 at the equator. The post-processed map of the Garnett et al., (2018) data is shown in Figure 1.

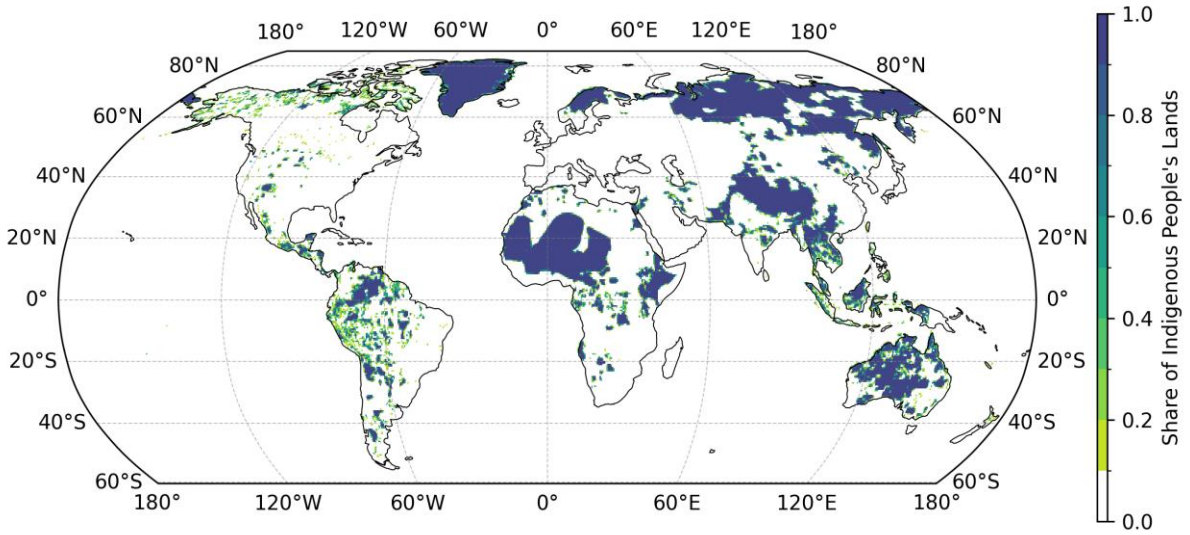

Figure 1: Global Map of IPL gridded at 0.5 deg and weighted by proportion of IPL per grid (e.g. 1 = 100% IPL within grid, 0.6 = 60% IPL within grid, 0 = no IPL within grid).

2.2 Exclusion of lands with negligible green water flow

Given the study's aim to understand the proportional contribution of IPL as a terrestrial precipitation source, the ratio of IPL to non-IPL globally could be an influential element of the analysis, if the performance of IPL lands was compared to non-IPL lands. As can be seen in Figure 1, there are substantial areas of permanent ice cover (e.g. the grids over Greenland) which are also grids with 100% IPL. While permanent ice areas do experience sublimation, the process by which snow evaporates directly into water vapour, this is not considered a green water flow. It is therefore common to exclude permanent ice areas from green water studies. There is also a high concentration of 100% IPL grids in arid areas with negligible ET (e.g. the grids over Sub-Saharan Africa), which could also disproportionally impact IPL performance in this study. We therefore chose to exclude terrestrial areas from this study that are characterised by permanent ice or extreme aridity (method described below), ensuring that the high proportion of these lands which are IPL will not factor into the analysis.

A green water flow criterion was identified as an objective basis for excluding land areas with negligible ET, using the ERA5 ET data which is used in the subsequent moisture tracking analysis (ERA5 is described in 3.1). We found areas of permanent ice and extreme aridity to be predominately below the 10th percentile of ET, which is 84 mm/year in the time period 2007-2018 (the

corresponding moisture tracking data time period). We therefore excluded all land areas in the moisture flow analysis with below the 10th percentile of ET.

The full distribution of terrestrial ET is shown in Figure 2, with IPL shown in shades of orange and non-IPL (i.e. all other land) shown in grey. The grids excluded from the analysis are below the 10th percentile of ET marked with a red dashed line, and make up 9.7 % of the global land area (Table 1). After application of the green water exclusion criterion, 15.3% of the total IPL global area and 7.8% of the total non-IPL global land area was removed. Figure 3 shows the terrestrial areas which are included in the study (both IPL and non-IPL) and their annual ET in mm/year; excluded land areas are shown in white, which includes the majority of Greenland and the Tibetan Plateau (areas of permanent ice), as well as the Sahara and the majority of the Arabian Peninsula (areas of extreme aridity). It is important to note that these excluded areas are only removed from the subsequent moisture flow analysis as sources of green water flow, they are not excluded as potential sink areas for TMR.

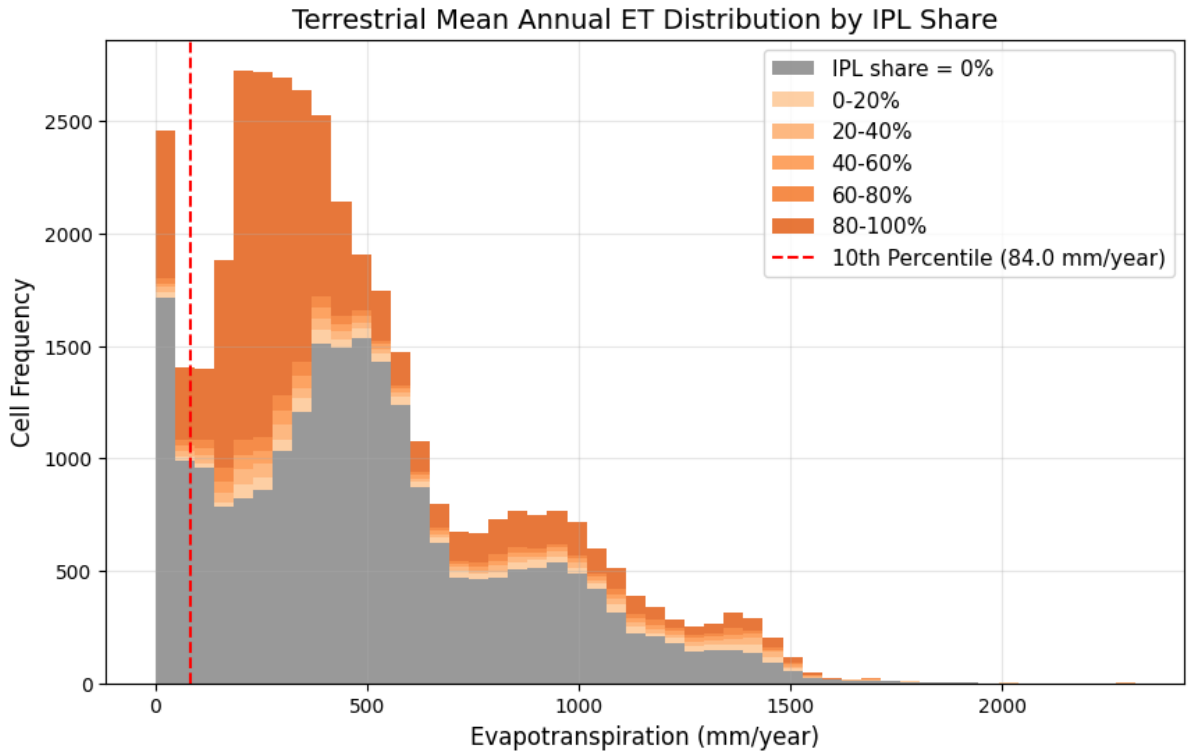

Figure 2: Distribution of terrestrial mean annual ET in the ERA5 dataset over the period 2007-2018, the 10th percentile (84 mm/year) is marked with a red dashed line.

Table 1: Summary of the initial and final terrestrial area for this study after excluding areas under the 10th percentile of ET.

Terrestrial Area	Initial Area		Removed Area		Final Area	
	[Million km³]	*[%]*	*[Million km³]*	*[%]*	*[Million km³]*	*[%]*
Global	147.2	100	14.3	9.7	120.2	100
IPL	37.2	25.3	5.7	15.3	31.5	26.2
Non-IPL	110	74.7	8.6	7.8	88.7	73.8

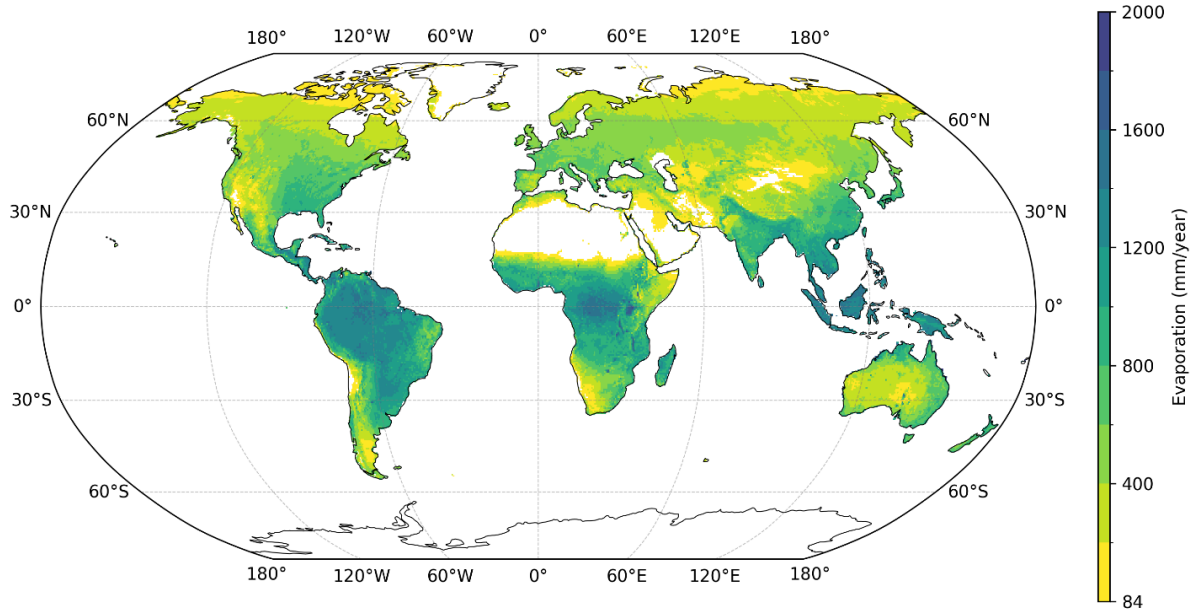

Figure 3: Land areas for inclusion in the moisture flow analysis (above the 10th percentile of ET [84 mm / year] in the ERA5 dataset over the period 2007-2018. Excluded land areas are depicted in white.

2.3 Mapped IPL for this study

Figure 4 provides a closer look at the remaining IPL areas for inclusion in the moisture flow analysis, and the proportion of IPL per grid. The darkest orange areas on the map are grids that are 100% IPL, and the lighter orange shades depict decreasing sub-grid % of IPL. The grey areas are either excluded land areas (the white areas of Figure 3) or included land areas with no IPL within the grid (the white areas of Figure 1). This map forms the basis of the subsequent moisture tracking analysis, where green water flow from IPL grids can be tracked from their source to the eventual sink of that moisture as precipitation on land or over the ocean.

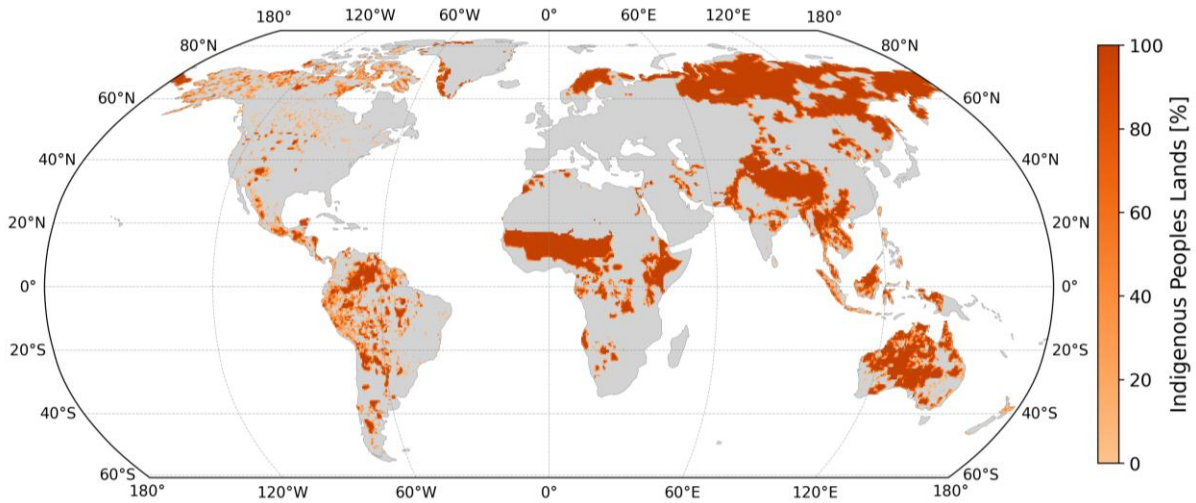

Figure 4: Global Map of IPL with ET > 84 mm/yr, for inclusion in the moisture flow analysis, gridded at 0.5 deg and weighted by proportion of IPL per grid.

3. Moisture Tracking Approach

3.1 The UTrack Model

This study tracks terrestrial moisture at the grid scale from its source as ET to its sink as precipitation utilising the UTrack moisture tracking dataset. UTrack is a state-of-the-art Lagrangian[3] atmospheric moisture tracking model (Staal et al., 2018; Tuinenburg & Staal, 2020) that traces moisture parcels from their evaporative origin to their precipitation destination and vice versa, at 0.5°x 0.5° resolution. The model is forced with ERA5 reanalysis data (European Centre for Medium-Range Weather Forecasts Reanalysis v5) (Hersbach et al., 2020), including wind speed, direction, and 25 vertical pressure layers, to resolve vertical shear in atmospheric moisture transport. Each parcel is tracked for 30 days or until 99% of its moisture content precipitates, according to the empirically-derived (ERA5) precipitation. To address uncertainties in vertical atmospheric shear, UTrack employs multiple vertical pressure layers from ERA5. The model handles uncertainties from parameterised processes, including convective updrafts and downdrafts, re-evaporation, and microphysical processes, through a probabilistic approach that randomly redistributes moisture parcels along the local vertical moisture profile every 24 hours. Although ERA5 exhibits known biases in tropical regions, UTrack's terrestrial moisture recycling simulations have been validated against seasonal tropical stable-isotope deuterium excess data (Cropper et al., 2021) and are internally consistent.

For this study, we utilise a dataset from a UTrack global simulation (i.e. every grid over land and ocean) over the period 2007 – 2018, aggregated to an annual timescale. The result is average moisture tracks per year from each grid on Earth, in the format of a data matrix of flows going in and out of each grid at each time-step. This dataset can be queried through post-processing steps called forward or backward tracking, where the flows can either be tracked forward from their source to their sink, or backward from their sink to their source.

3.2 Conceptual Approach

An **evaporationshed** describes the downwind atmosphere and surface (ocean and land) that receives precipitation from a specific location's evaporation, whose extent is shaped by prevailing wind fields and atmospheric circulation patterns (van der Ent & Savenije, 2013). Figure 5 depicts the evaporationshed concept, where the gridded terrestrial area is a hypothetical area of interest, i.e. the source of green water flow, from which moisture is tracked downwind (forward tracking) to its terrestrial or oceanic destination (sink area) as precipitation. The concept could also be thought of as a green water flow footprint. In contrast to watersheds (river basins / catchments) where the boundaries are deterministically defined by topographic features and soil properties, the boundaries of evaporationsheds are probabilistic, referring to an ensemble- or time-averaged potential trajectory of an atmospheric water parcel.

3 Lagrangian models describe the motion of systems by tracking paths of individual particles or points, as opposed to a Eulerian model of overall flow fields on a fixed grid.

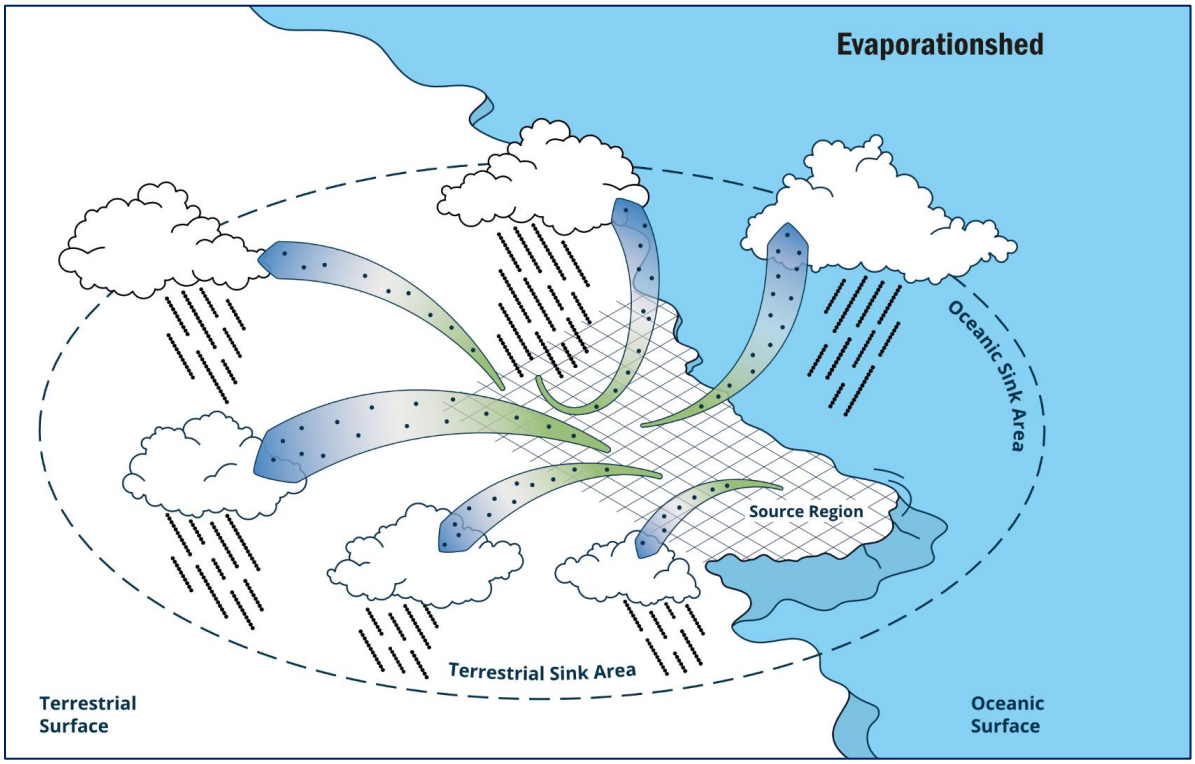

Figure 5: Conceptual diagram of an evaporationshed. Source: GCEW 2024

The IPL map in Figure 4 provides the IPL grids from which moisture can be forward tracked to its eventual sink. The proportion of IPL per grid can be used as a weight to scale the amount of green water flow from each grid, allowing for a more accurate estimate. Figure 6 (next page) depicts this study's concept for tracking moisture from IPL grids, where the green water flow is weighted by the corresponding proportion of IPL with that grid, and only this moisture is forward tracked in the moisture flow network. In this way, we can isolate the IPL contribution to precipitation in a given sink grid. We additionally perform a baseline scenario of moisture flows from all lands globally so comparison is possible between IPL and non-IPL. The difference between precipitation at each grid in the baseline scenario of all flows from all grids and the IPL scenario effectively isolates the moisture contribution of non-IPL grids.

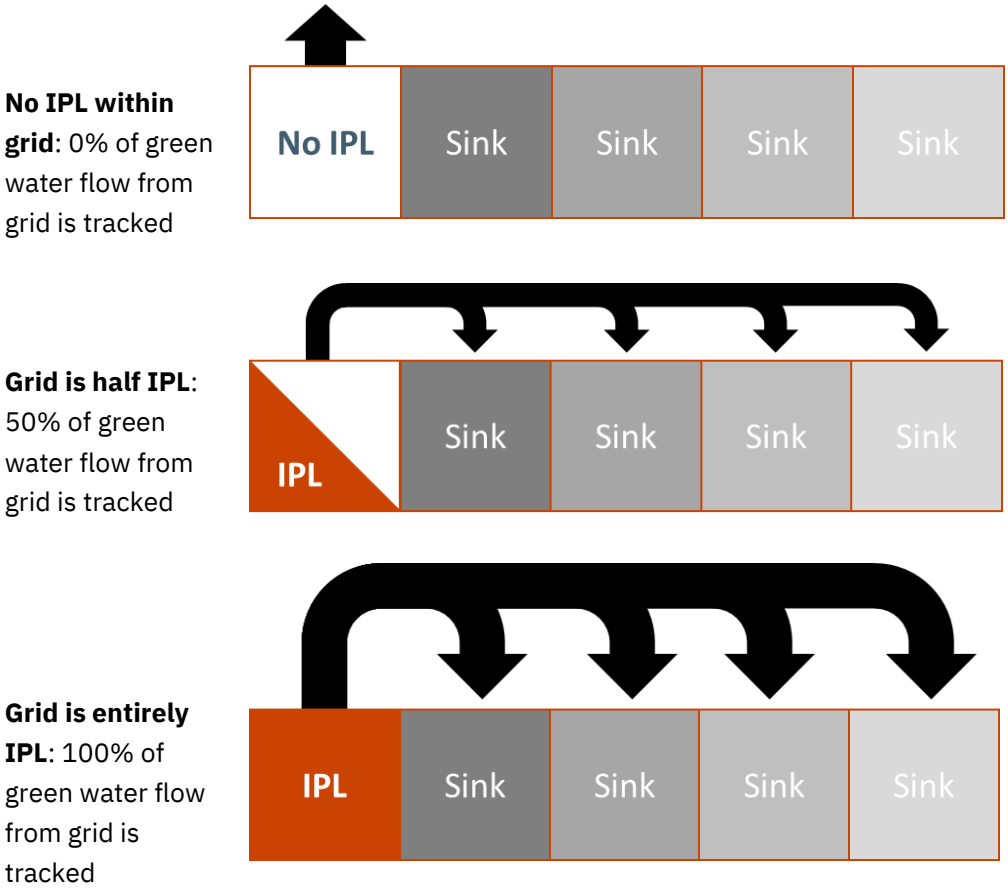

Figure 6: Conceptual diagram of green water flow from IPL grids, where the proportion of IPL per grid weights the green water flow for moisture tracking. In the top panel, there is no IPL within the source grid, so no moisture is tracked. In the middle panel and bottom panels, 50% and 100% of the source grids moisture is tracked, corresponding to the IPL proportion.

4. Analysis

4.1 The evaporationshed of global IPL

Deriving the evaporationshed of IPL globally from the moisture flow data is an analysis which shows the full reach of IPL green water flow, including the amount of moisture which reaches each sink grid as precipitation. The evaporationshed of IPL globally, over the period 2007-2018, was delineated by forward tracking moisture from all IPL grids, summing the precipitation contribution annually and then averaging over the period. Figure 7 maps the spatial extent of the global IPL evaporationshed (over terrestrial and oceanic surface) shown with the amount of precipitation in mm/yr. This can be interpreted as the amount of green water flow from IPL source grids contributed to each sink grid.

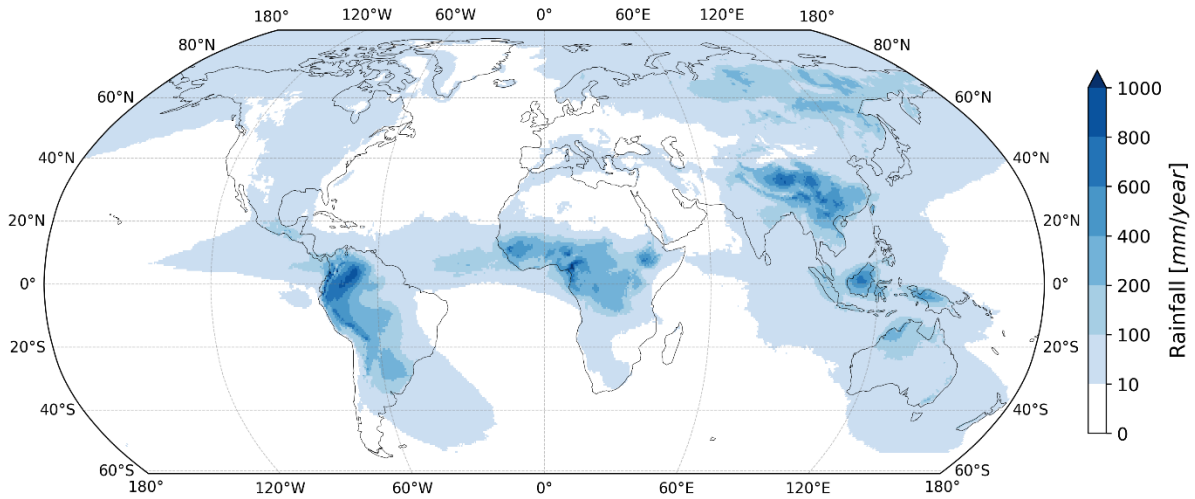

Figure 7: The global IPL evaporationshed spatial extent depicted with amount of precipitation (mm/year) contributed from IPL green water flow (average annual over the period 2007-2018).

There are large swaths of the terrestrial and ocean surface that receive relatively small moisture contributions from IPL (< 100 mm/year; light blue areas in Figure 7). The vast global reach of IPL moisture makes sense given the presence of IPL on all inhabited continents. There is even shown to be a transatlantic teleconnection of IPL moisture from Africa to South America. Parts of southern South America, northern Australia and the boreal region in Russia emerge as receiving moderately high amounts of IPL moisture (> 400 mm/year; mid-blue shades in Figure 7). There are clear hotspots which receive the largest amounts of precipitation from IPL moisture (> 800 mm/year; dark blue areas in Figure 7) – namely northeast South America, Central Africa, Southeast Asia, the Tibetan Plateau and the Indonesian Archipelago. These identified hotspots coincide with known TMR hubs (Keys, 2016; Wunderling et al., 2022), areas which exhibit a tight coupling between the terrestrial source and terrestrial sink of moisture flows, usually due to topographical controls on precipitation, such as mountain ranges, in combination with prevailing wind patterns. It therefore makes sense that regions which are already known to recycle a lot of terrestrial moisture would also recycle a lot of IPL moisture.

To understand the seasonality of the global IPL evaporationshed, a monthly analysis was performed by forward tracking moisture from all IPL grids (as above), summing the precipitation contribution each month and then averaging over the period (2007-2018). Figure 8 shows the 12 monthly global IPL evaporationsheds. To animate the progression of changes in the spatial extent and precipitation amounts, the monthly evaporationsheds have been compiled into a GIF looping through the months (file provided digitally upon request). Here in Figure 8 we display the individual months (which make up the GIF) in a small size for space considerations (full resolution images provided digitally upon request).

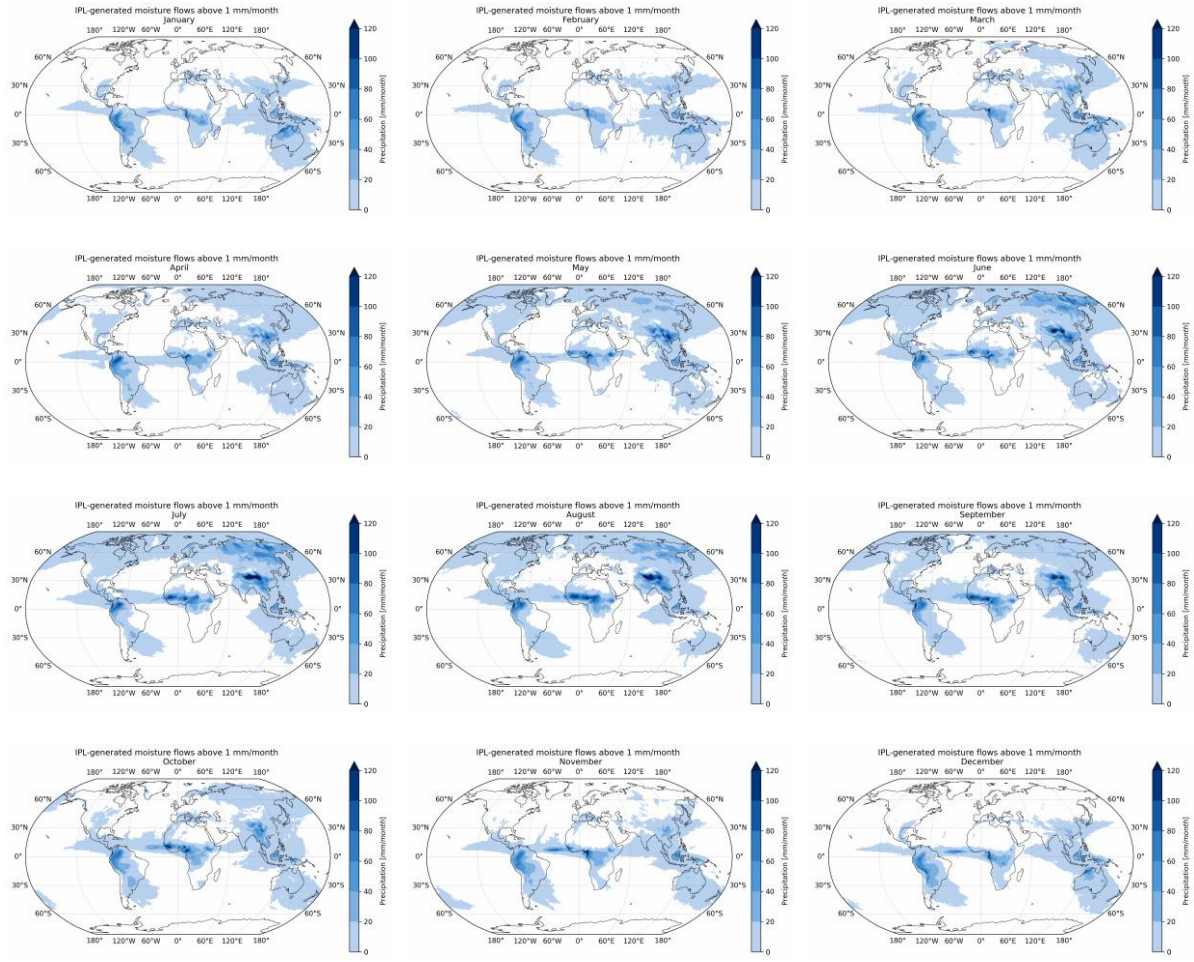

Figure 8: The global IPL monthly evaporationshed spatial extents depicted with amount of precipitation (mm/month) contributed from IPL green water flow (average monthly over the period 2007-2018). Precipitation < 1 mm/month is not displayed. Full resolution images are provided along with a GIF which loops through these maps to show the monthly progression of the IPL evaporationshed.

Seasonal changes in atmospheric circulation and temperature result in noticeable differences in the spatial extents of the IPL evaporationshed throughout the year. From May – September the IPL evaporationshed is at its most expansive, reaching the northern latitudes, while from November – February the IPL evaporationshed is mostly contained to mid and southern latitudes. Increased ET rates in the summer months adds more green water to the moisture flow network and explains the higher expansion into the boreal zone. In the tropics and subtropics, patterns reflect the shifting of

the Intertropical Convergence Zone (ITCZ) and seasonal monsoon behaviour are most prominent. Throughout the year, the ITCZ essentially migrates to the latitudes with the highest solar heating, shifting southward in the Northern Hemisphere winter. This large-scale convective displacement not only shuts down the summer monsoons in the Northern Hemisphere, but delivers heavy rainfall to the tropics in the Southern Hemisphere. In summary, the seasonal patterns in IPL moisture transport are following the same patterns which are known to influence the transport of all terrestrially sourced moisture.

4.2 Global contribution of IPL to terrestrial moisture flows

While the evaporationshed analysis (Section 4.1) shows the extent and amount of IPL moisture sinks, allowing for relative comparisons of IPL-sourced precipitation across regions, it does not reveal the relative importance of the IPL-sourced moisture to the total. Going forward in the analysis, there are two options in terms of defining total precipitation (of a grid)- either it is the sum of all moisture sources (ocean + IPL + non-IPL) or it is focused only on terrestrial moisture sources (IPL + non-IPL). A focus on terrestrially-sourced moisture concerns land / vegetation regulated green water flows whereas the ocean contribution to terrestrial precipitation is regulated by large scale circulation patterns, seasonal cycles and climate. Given the limited capacity of this study, and the ultimate aim of connecting these results to forms of land stewardship, we choose to focus on terrestrially-sourced moisture only, in terms of the IPL relative contribution.

To assess the contribution of IPL among all terrestrially-sourced moisture in the flow network, we next set out to quantify the volumes and recycling ratios of IPL green water flow as compared to non-IPL. Of the land area included in the analysis, we find that the ET from all lands globally source moisture which generates 76,752 km^3/year of precipitation, of which 53,898 km^3/year precipitates on land and 22,854 km^3/year precipitates over the ocean.

Table 2. Summary of terrestrially-generated precipitation sources (all land, Non-IPL, IPL) and their sinks (land, ocean)

Terrestrially sourced moisture		Land	Ocean	Total
All lands *[km^3/year]*	*Vol*	53,898	22,854	76,752
	ET recycling ratio	*70%*		
Non-IPL *[km^3/year]*	*Vol*	40,895	17,710	58,605
	ET recycling ratio	*70%*		
IPL *[km^3/year]*	*Vol*	13,003	5,144	18,147
	ET recycling ratio	*72%*		

For this study, all terrestrial land is considered either as IPL or non-IPL. Due to its larger share of the global land area (73.8%, Table 1), non-IPL green water flow sources a higher amount of precipitation (40,895 km^3/year, Table 2) as compared to IPL on 26.2% of the global land area (Table 1) which generates 13,003 km^3/year of precipitation (Table 2).

One measure of performance could be to consider the proportion of terrestrial precipitation generated given the proportion of terrestrial land. This analysis finds that IPL are generating 24.1% of terrestrially-sourced precipitation from 26.2% of the global land area, and non-IPL are generating 75.9% of terrestrially-sourced precipitation from 73.8% of the global land area. Even though IPL's precipitation generation share is lower than its land share (and non-IPL's is higher), this should not be interpreted as an out-performance of non-IPL to IPL as these differences are simply too slight given the limitations and uncertainties associated with modelling moisture flows. Rather, the main takeaway is that IPL and non-IPL are both generating terrestrial precipitation proportional to their relative share of land globally. Since this measure is essentially scaling by the land share proportion, it is not revealing any differences in land use / land cover on IPL which impact TMR.

Another measure of performance could be to consider the amount of green water flow (ET) which recycles on land, the so-called ET recycling ratio. Globally, all lands have an ET recycling ratio of 70%, where the remaining 30% precipitates over the ocean. Of these lands, the IPL ET recycling ratio is 72% (and 28% precipitates over the ocean) and the non-IPL ET recycling ratio is 70% (and 30% precipitates into the ocean) (Table 2). Even though IPL's ET recycling ratio is higher than non-IPL's, we do not interpret this as an out-performance if IPL to non-IPL as these differences are too slight given the limitations and uncertainties associated with modelling moisture flows. Rather, the main takeaway is that IPL and non-IPL are recycling essentially the same proportion of their green water flow on land. This measure also does not reveal any possible differences in land use / land cover on IPL which impact TMR.

4.3 Terrestrial moisture recycling over IPL

Deriving the TMR ratios from IPL globally is an analysis which shows the proportion each sink grid is receiving in terms of IPL moisture contribution to its precipitation. This mapping exercise reveals the regions which are most dependent on IPL green water flow for their terrestrially-sourced precipitation. Figure 9 shows the proportion of terrestrially-sourced moisture that comes from IPL, where areas depicted in white receive no IPL moisture and areas depicted in darker purple receive more of their terrestrially sourced precipitation from IPL. Notably, there are parts of world receiving over 60% of their land sourced precipitation from IPL with some clusters of grids in West Africa and the Tibetan Plateau receiving over 80% (Figure 9).

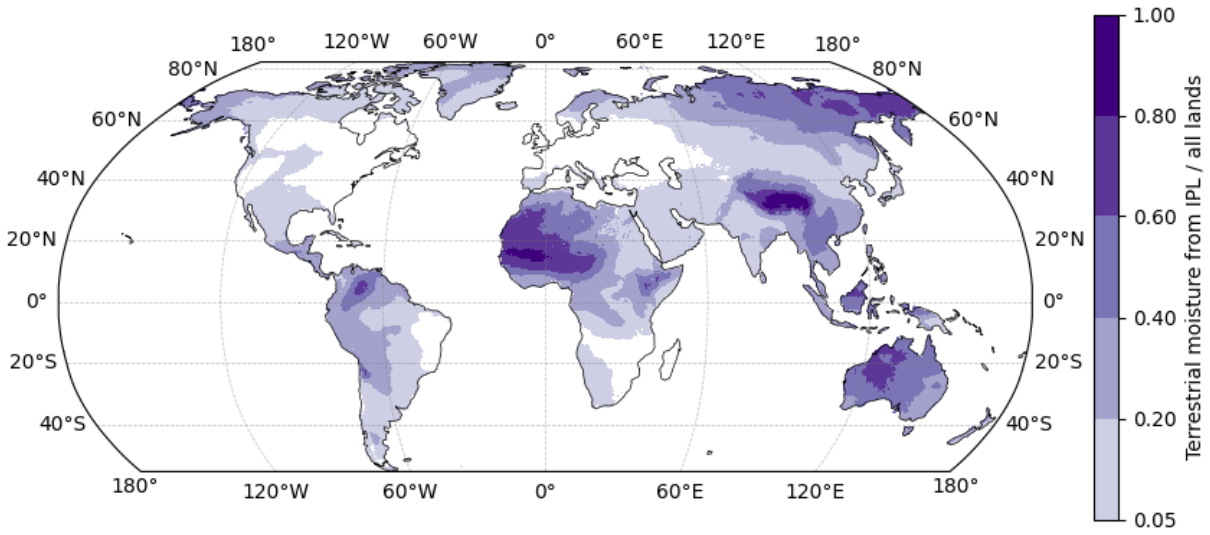

Figure 9: The proportion of terrestrially-sourced precipitation from IPL. Notably, some regions rely on IPL for over 80% of their terrestrially-sourced precipitation (dark purple).

Table 3: Summary of IPL moisture inputs by continent. The total IPL moisture received in km³/year reflects the moisture input to each continent from IPL globally. IPL to IPL / non-IPL moisture recycling reflects the amount and proportion of IPL moisture globally which recycles on IPL / non-IPL on each continent, reported in both amount (km³/year) and proportion (%).

Continent	**Total IPL moisture received** (km³/year)	**IPL to IPL moisture recycling**		**IPL to non-IPL moisture recycling**	
		(km³/year)	(%)	(km³/year)	(%)
South America	3325.76	2106.93	63.35%	1218.83	36.65%
North America	243.13	63.24	26.01%	179.85	73.98%
Africa	3133.66	1794.93	57.28%	1338.73	42.72%
Asia	5149.05	3596.78	69.85%	1552.27	30.15%
Australia & Oceania	617.93	481.36	77.90%	136.47	22.09%
Europe	147.94	52.82	35.71%	95.14	64.31%

Table 3 provides a continental analysis which breaks down the amount of IPL moisture from all lands globally which contribute to precipitation (moisture sink) on each continent. Here, IPL to IPL moisture recycling indicates green water flow from all IPL globally which terrestrially recycles on IPL on a given continent, and IPL to non-IPL moisture recycling indicates green water flow from all IPL globally which terrestrially recycles on non-IPL on a given continent. The Asian continent receives the highest volume of global IPL moisture (5149.05 km³/year), as well as the highest volume on its IPL and its non-IPL (Table 3). Australia & Oceania has the highest proportion of IPL to IPL moisture recycling (77.9%) and North America has the highest proportion of IPL to non-IPL moisture recycling (73.98%).

4.4 Regional and dry season analysis

To provide more insight into the contribution of IPL green water flow to terrestrial precipitation, it was decided with the SIWI colleagues that a sub-global and sub-annual scale analysis would be beneficial. First, we plotted a latitudinal view of mean seasonal terrestrial precipitation generated from IPL to show these nuances (Figure 10).

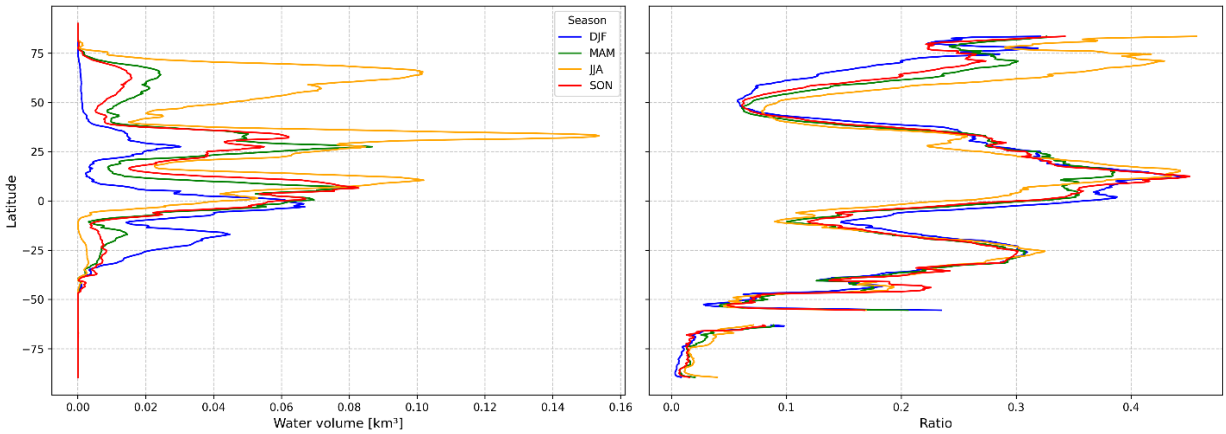

Figure 10: IPL moisture destinations according to latitude and season by volume (left panel) and by TMR ratio (right panel). The gap at 60°S is due to the fact that there are no lands at this latitude.

The aim of this exercise was to get a first glimpse magnitude of sub-global and sub-annual scales differences ahead of undertaking further analysis. The left panel of Figure 10 shows the volume of precipitation (km^3) generated by IPL and the right panel shows the TMR ratio of IPL to all lands, both are per season and by latitude, taken together, this information shows both the absolute amount and the relative importance, respectively. IPL are contributing the largest volumes of moisture in the Northern Hemisphere in June/July/August (JJA) and have a relatively high contribution in the Southern Hemisphere in December/January/February (DJF). Despite the fluctuations in volume of moisture, the TMR ratios follow a more consistent pattern latitudinally, though regional differences within a latitudinal band are hidden.

Moving forward with a regional scale analysis, we first had to choose a region mask fit for purpose. In Giorgi & Francisco (2000), 21 large-scale reference regions were created on global land areas (except Antarctica) for the purpose of regional climate analysis. The so-called Giorgi regions are commonly used by the IPCC and many other regional studies, making them ideal for use in this study as well. Figure 11 maps these defined regions, which are either at sub-continental or continental-scale. Note that the region masks include both land and ocean areas; for this study we only consider the terrestrial area of each Giorgi region.

The 21 Giorgi regions are assigned a three-letter abbreviation as follows (listed alphabetically):

ALA – Alaska
AMZ – Amazon
AUS – Australia
CAM – Central America
CAS – Central Asia
CAN – Central North Africa
EAF – East Africa
EAS – East Asia
ENA – Eastern North America
GRL – Greenland
MED – Mediterranean
NAS – Northern Asia
NEU – Northern Europe
SAF – Southern Africa
SAH – Sahara
SAS – South Asia
SEA – Southeast Asia
SSA – Southern South America
TIB – Tibetan Plateau
WAF – West Africa
WNA – Western North America

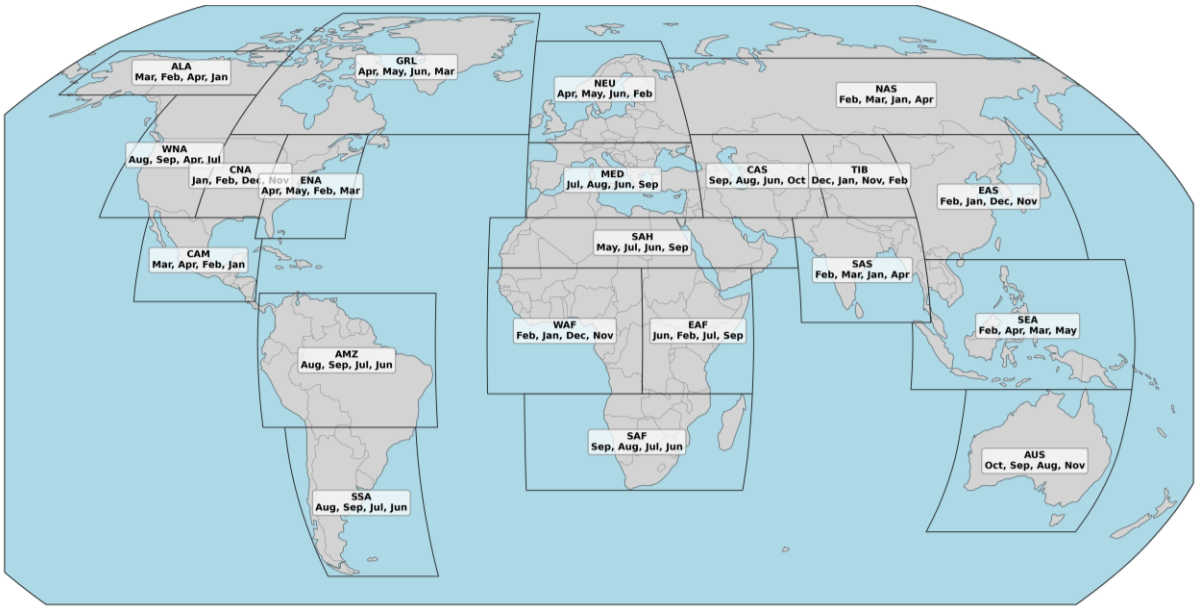

Figure 11: The 21 Giorgi regions commonly used for regional climate analysis, displayed with their dry season months defined as the driest four months over the period 2007-2018 in ERA5 precipitation.

Figure 9 in section 4.3 already displays the proportion of terrestrially-sourced precipitation from IPL for each grid in our study. Now using the Giorgi regions, we can aggregate this information to provide regional estimates (Table 4). Much of the IPL sources are likely from with each region itself, though it can also come from IPL in other regions. The regional aggregation only constrains the sink region, not the source region.

Table 4 reports the regional values which breaks down the amount of IPL moisture from all lands globally which contribute to precipitation (moisture sink) in each region. Here, IPL to IPL moisture recycling indicates green water flow from all IPL globally which terrestrially recycles on IPL in a given region, and IPL to non-IPL moisture recycling indicates green water flow from all IPL globally which terrestrially recycles on non-IPL in a given region. The most highly dependent regions on IPL moisture for their terrestrially sourced precipitation are Australia (48%), West Africa (40%), Southeast Asia (37%) and the Tibetan Plateau (37%).

Table 4: Summary of IPL moisture inputs to each Giorgi Region. The total IPL moisture received in km³/year reflects the moisture input to each region from IPL globally. The IPL proportion of that reflects the share of IPL moisture given the total terrestrially sourced moisture. The IPL to IPL / non-IPL moisture recycling reflects the amount and proportion of IPL moisture globally which recycles on IPL / non-IPL in each region, reported in both amount (km³/year) and proportion (%).

Region		**Total IPL moisture received** (km³/year)	**IPL proportion of terrestrially-sourced moisture** (%)	**IPL to IPL moisture recycling**		**IPL to non-IPL moisture recycling**	
Giorgi Abv.	Name			(km³/year)	(%)	(km³/year)	(%)
ALA	Alaska	94.32	14.3	42.66	45.23	51.66	54.77
AMZ	Amazon Basin	2749.64	21.4	1884.86	68.55	867.83	31.56
AUS	Australia	617.93	47.9	481.27	77.88	136.67	22.12
CAM	Central America	137.68	18.9	93.09	67.61	44.31	32.19
CAS	Central Asia	131.74	8.57	49.17	37.32	82.57	62.68
CNA	Central North America	65.30	5.02	6.79	10.40	58.51	89.60
EAF	East Africa	940.42	20.35	419.02	44.56	521.40	55.44
EAS	East Asia	1289.99	25.07	627.23	48.62	662.76	51.38
ENA	Eastern North America	25.67	2.57	2.21	8.62	23.46	91.38
GRL	Greenland	91.23	17.95	41.69	45.70	49.54	54.30
MED	Mediterranean	64.52	10.61	10.22	15.84	54.30	84.16
NAS	North Asia	1495.12	26.23	1109.55	74.21	383.95	25.68
NEU	Northern Europe	83.46	7.43	42.65	51.10	40.81	48.90
SAF	Southern Africa	94.41	3.86	13.87	14.70	80.43	85.19
SAH	Sahara	48.76	26.25	32.08	65.78	16.69	34.22
SAS	South Asia	642.80	24.52	466.01	72.50	176.79	27.50
SEA	Southeast Asia	787.67	37.33	629.41	79.91	158.26	20.09
SSA	Southern South America	575.80	14.73	223.64	38.84	352.16	61.16
TIB	Tibetan Plateau	802.80	36.82	716.10	89.20	86.70	10.80
WAF	West Africa	2049.51	40.21	1329.54	64.87	719.97	35.13
WNA	Western North America	57.83	4.79	11.64	20.13	46.19	79.87

For the seasonal analysis, we prioritised the dry season of each region, where understanding and securing precipitation sources are critical (given the limited capacity of this project). We defined the dry season as the four driest months (not necessarily consecutive) in each region over period 2007-2018 in ERA5 precipitation. Figure 11 displays the four driest months for each Giorgi region.

Figure 12 (below) packages our regional analysis for each Giorgi region. The left panel shows the IPL sourced moisture per month both in terms of volume (km³, blue line) and percentage of terrestrially sourced moisture (purple line). The dry season is indicated by the months shaded in grey, usually these are consecutive months, though sometimes not. The right panel displays the proportion of

terrestrially-sourced precipitation from IPL for each grid within a map view cropped to the Giorgi region; the regional average ratios of (all grids in) each region are reported in Table 4.

a) ALA

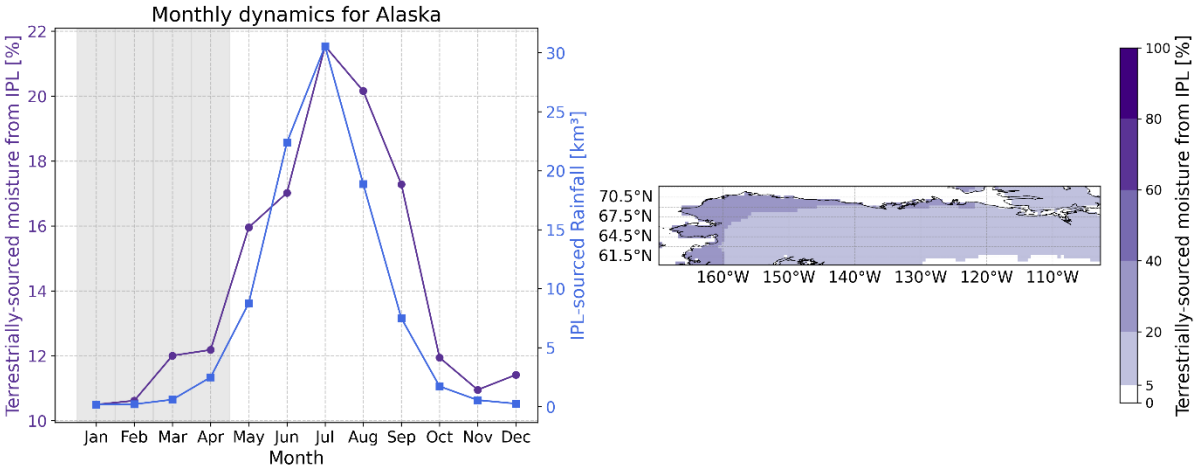

b) AMZ

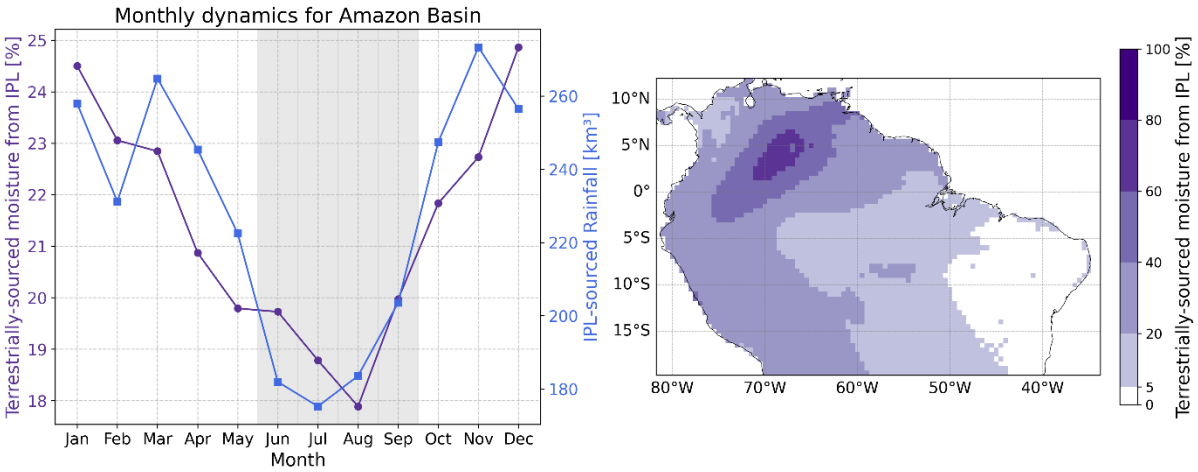

c) AUS

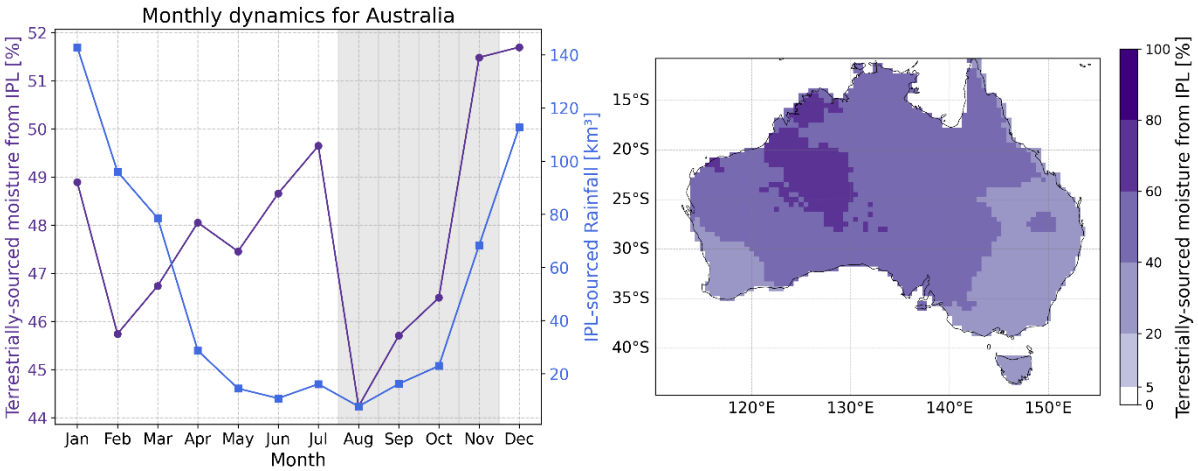

d) CAM

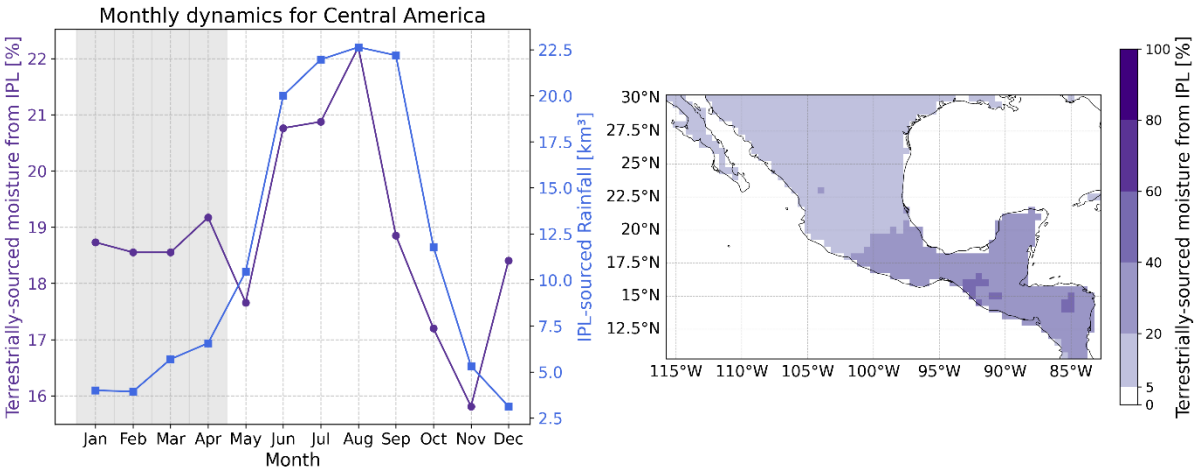

e) CAS

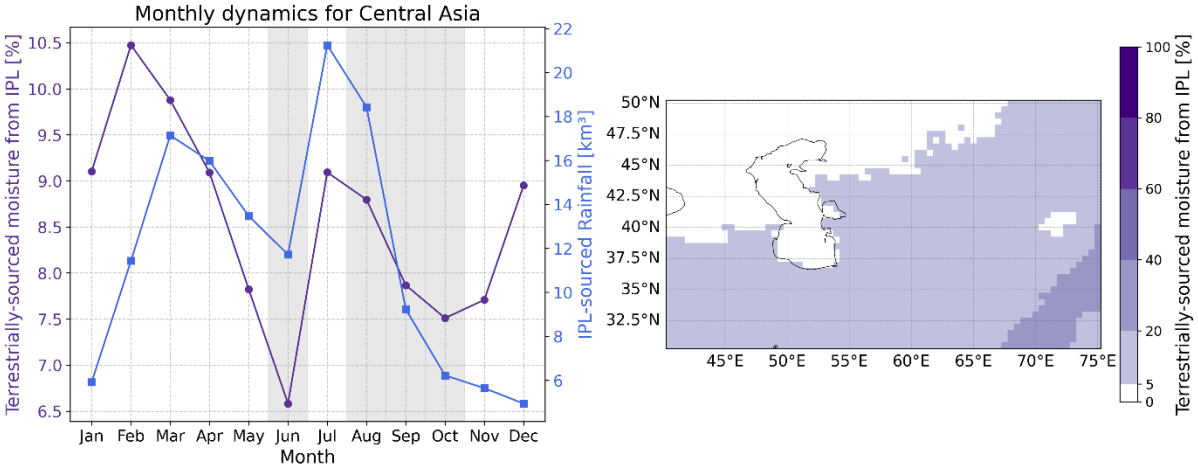

f) CNA

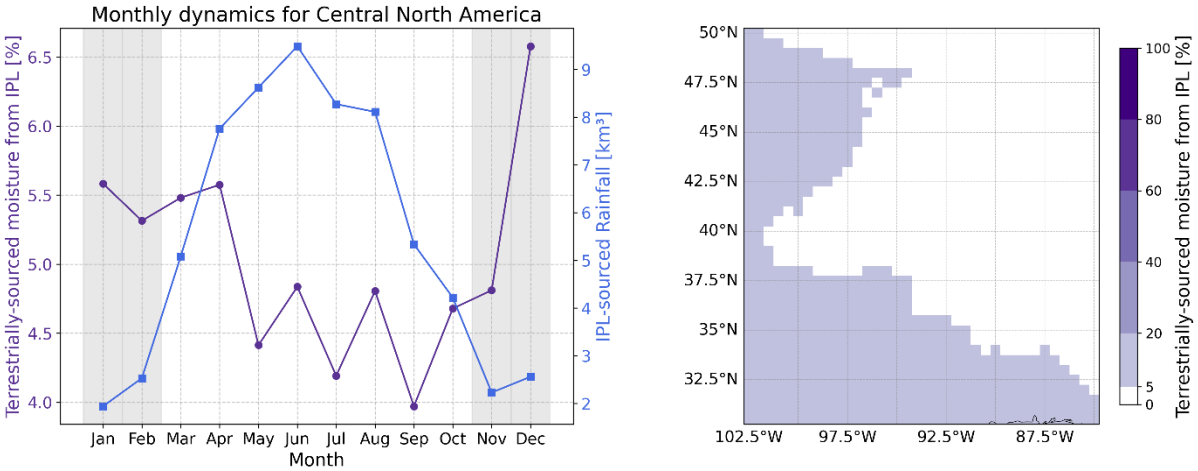

g) EAF

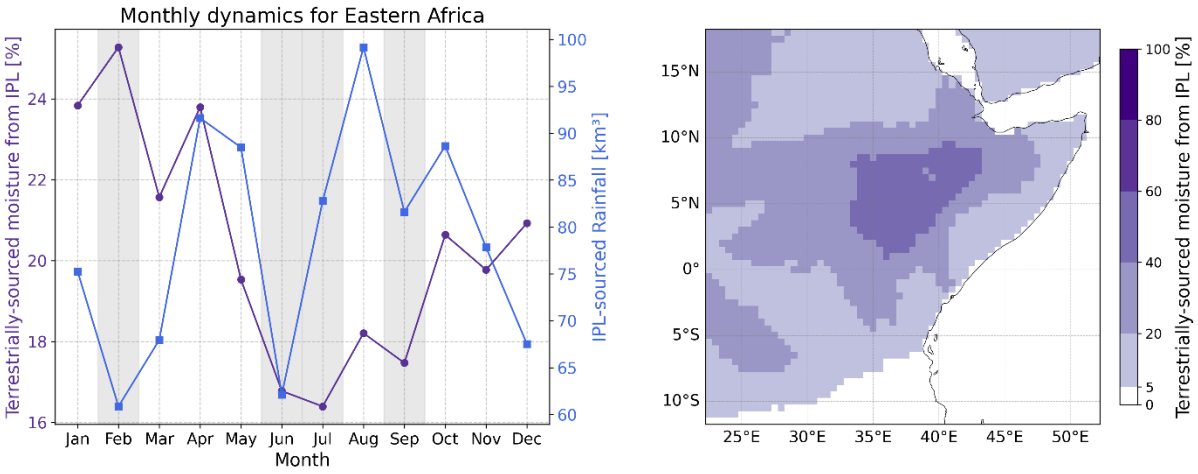

h) EAS

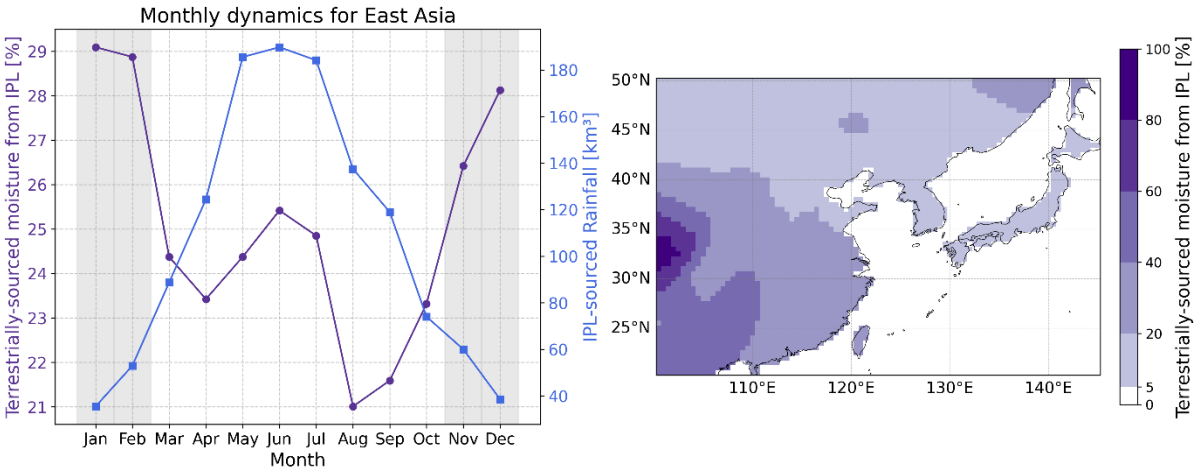

i) ENA

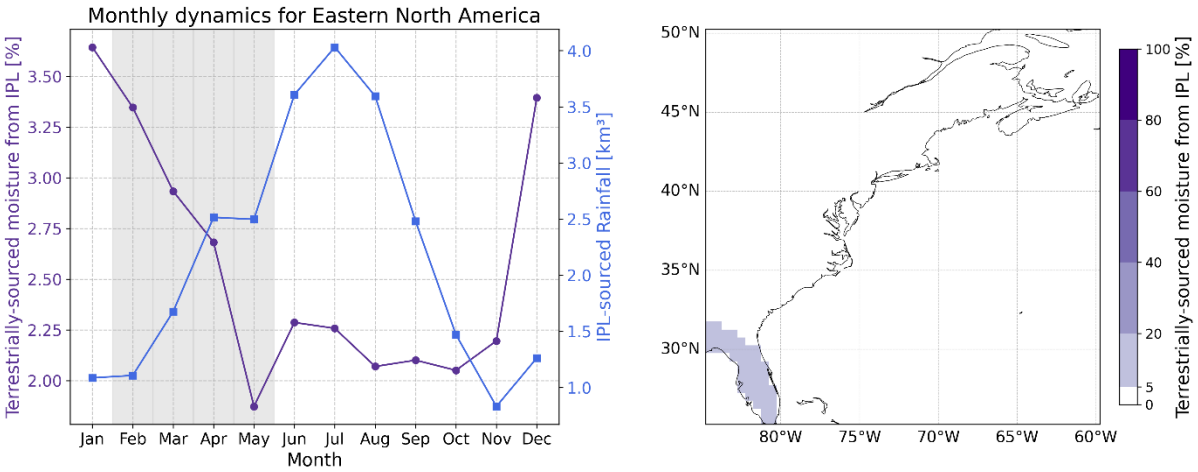

j) GRL

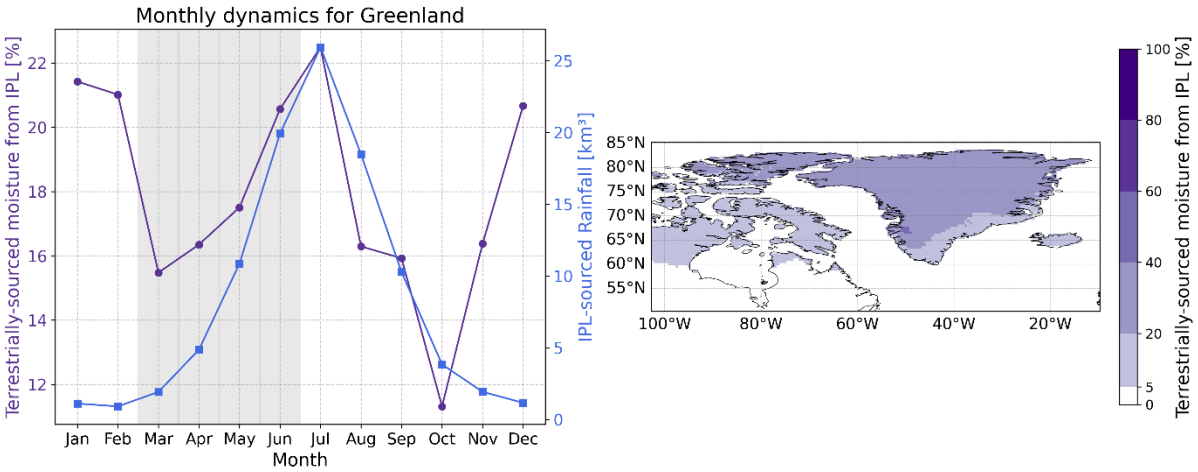

k) MED

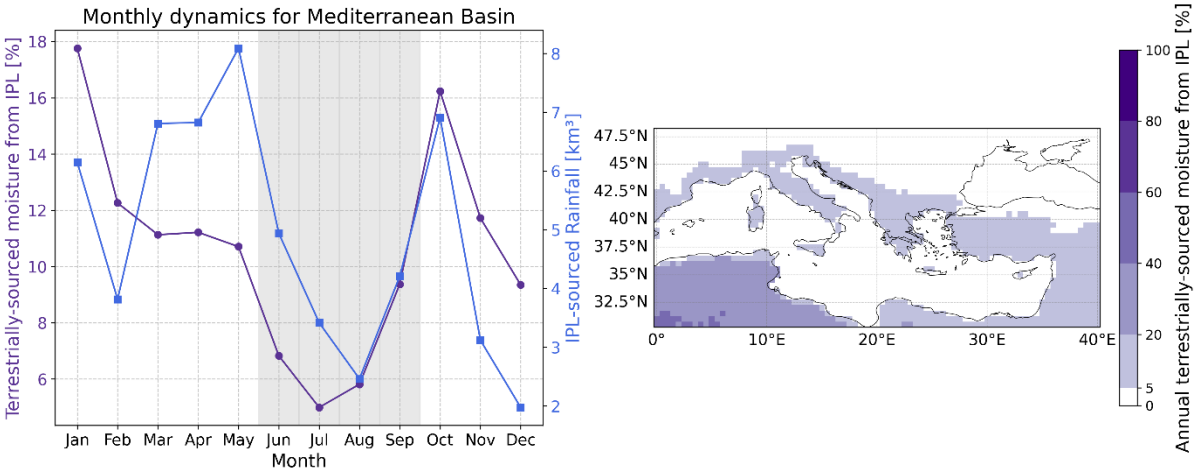

l) NAS

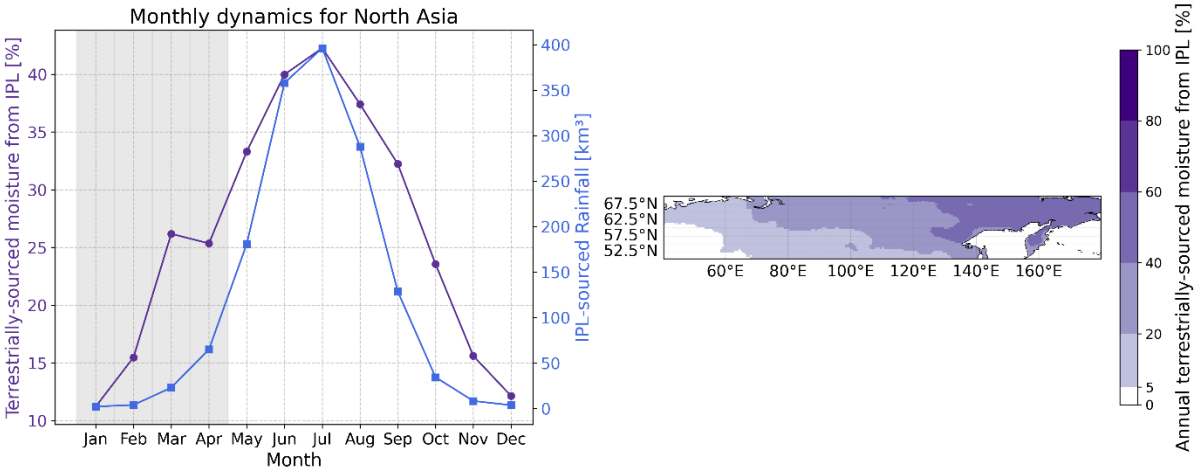

m) NEW

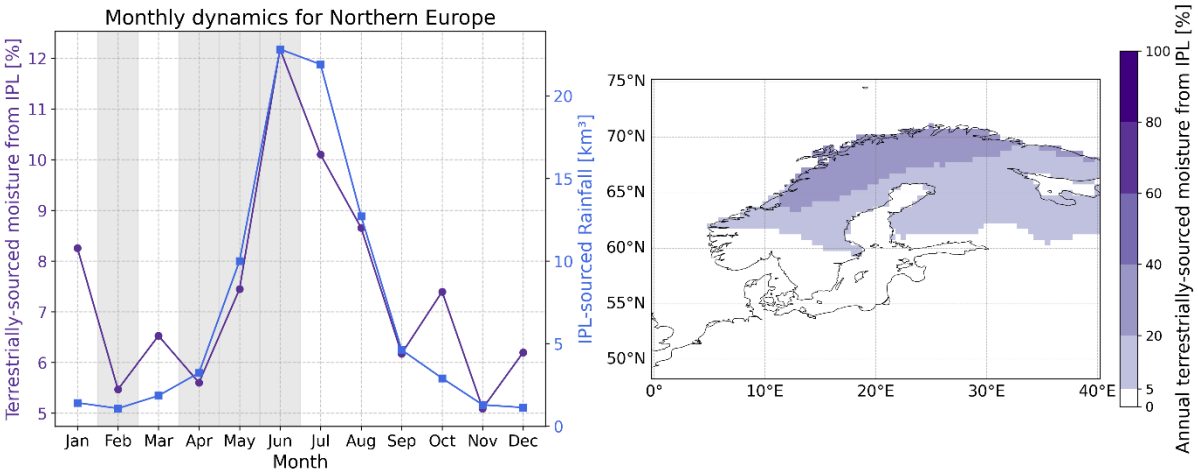

n) SAF

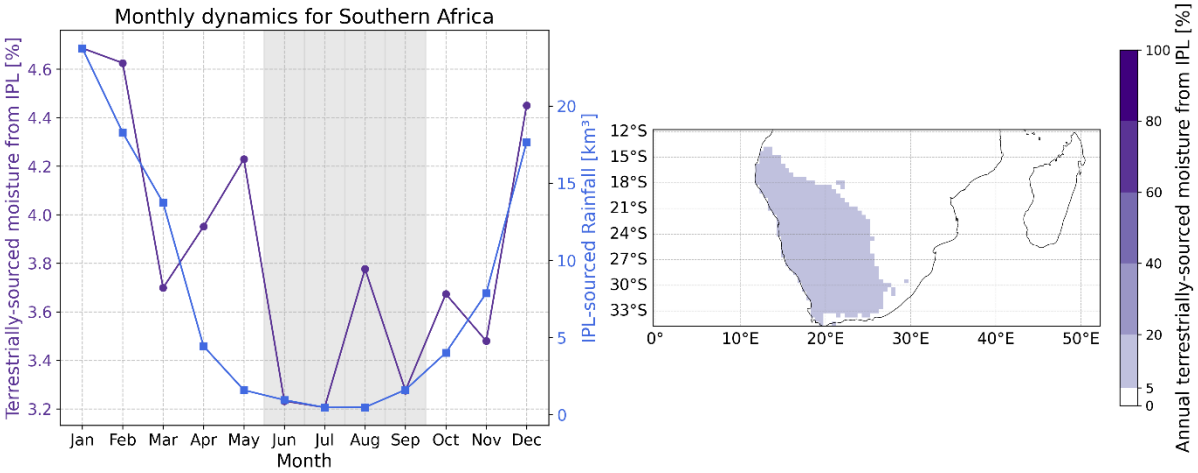

o) SAH

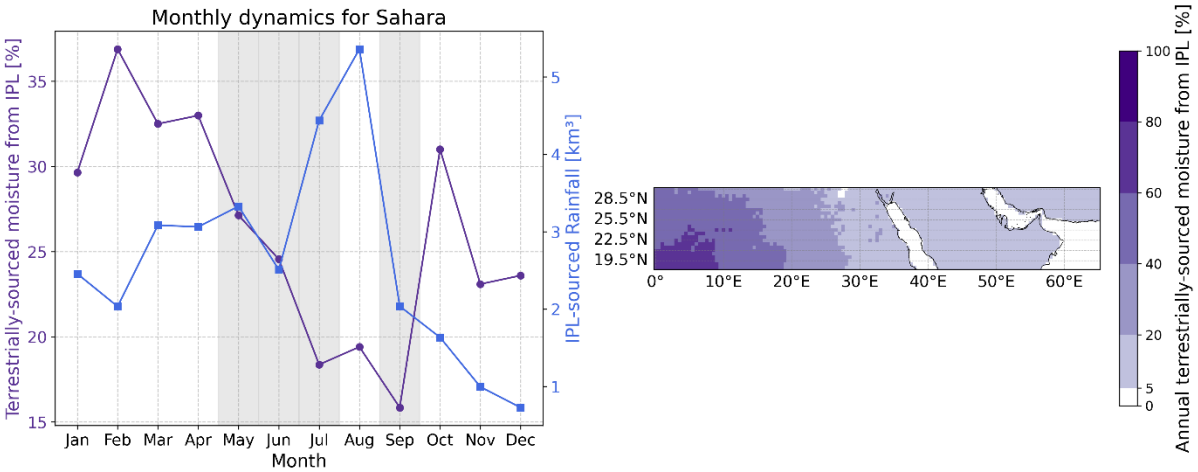

p) SAS

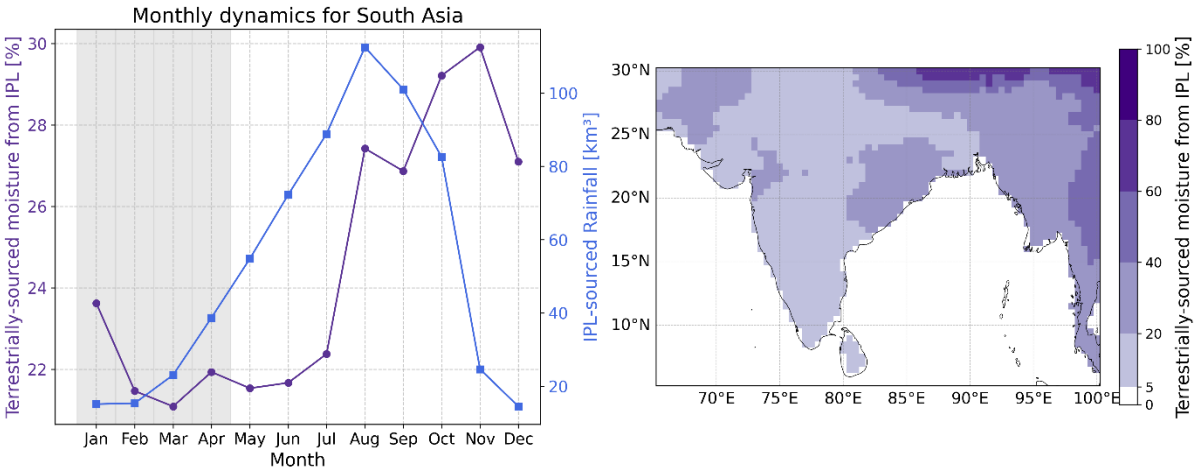

q) SEA

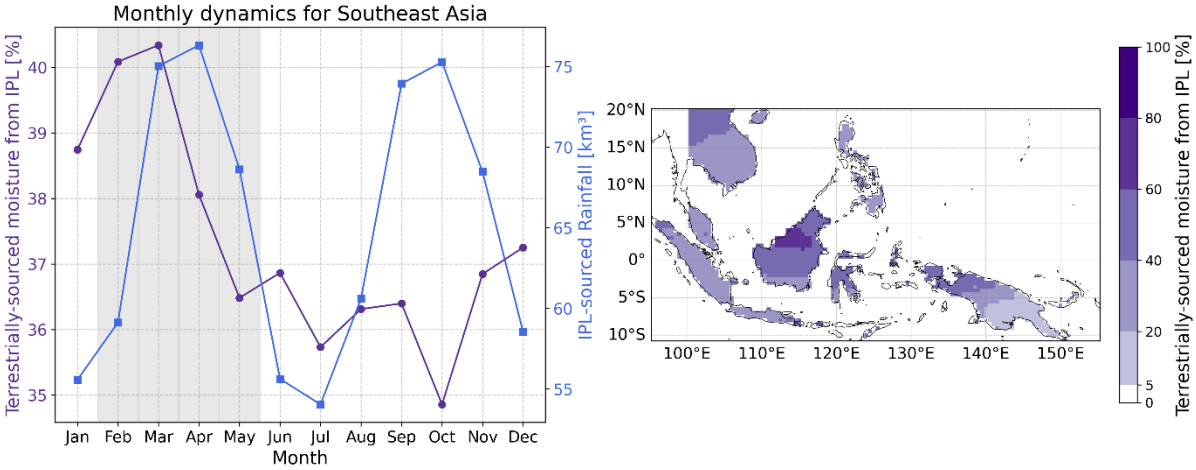

r) SSA

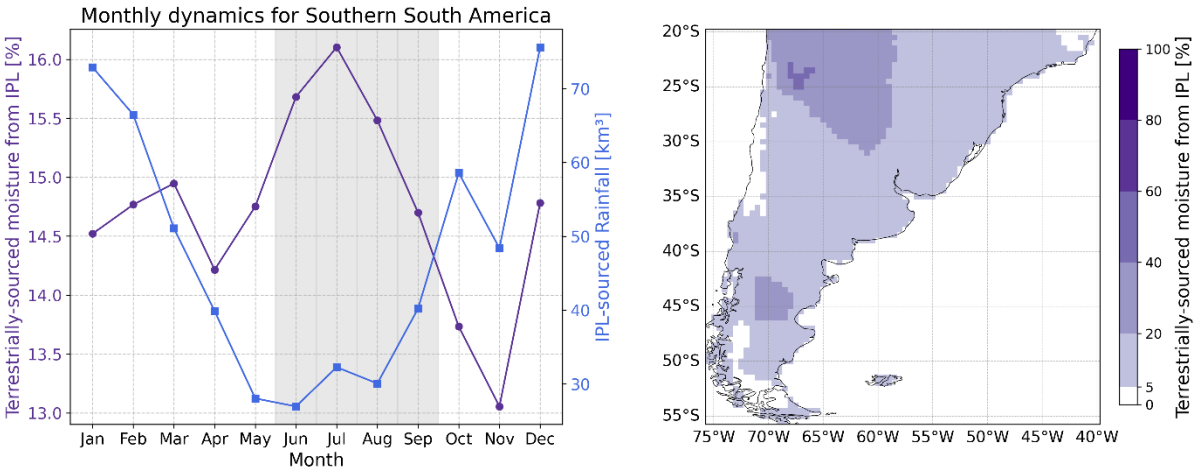

s) TIB

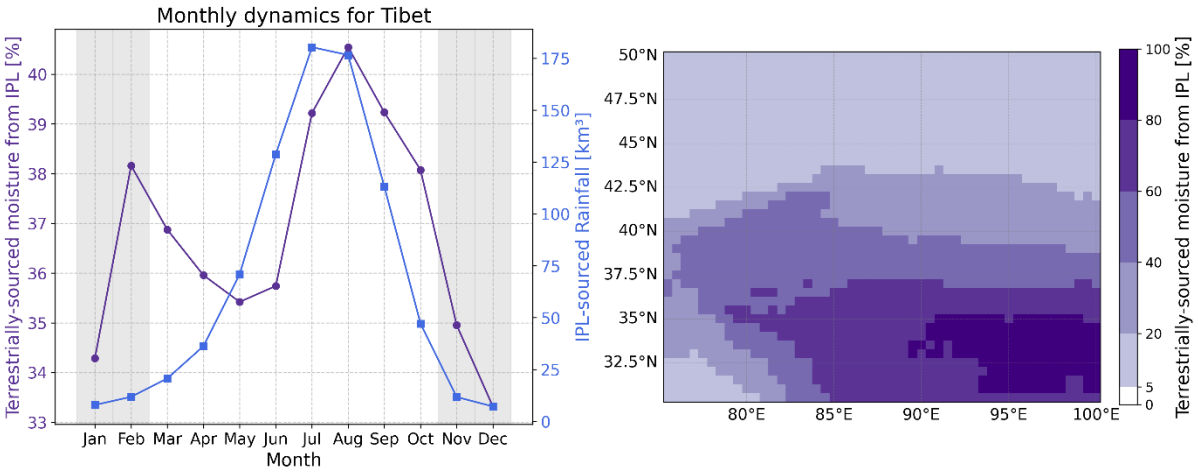

t) WAF

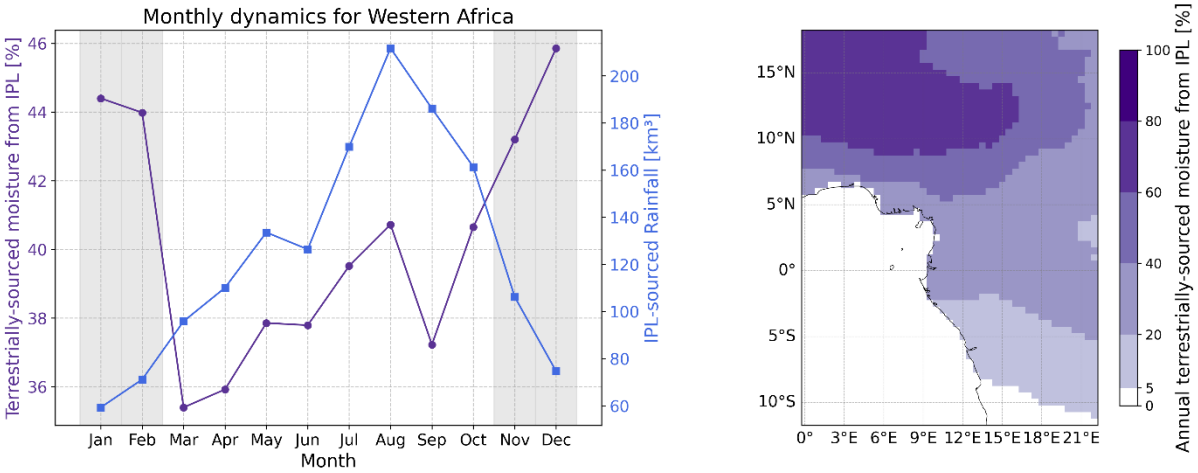

u) WNA

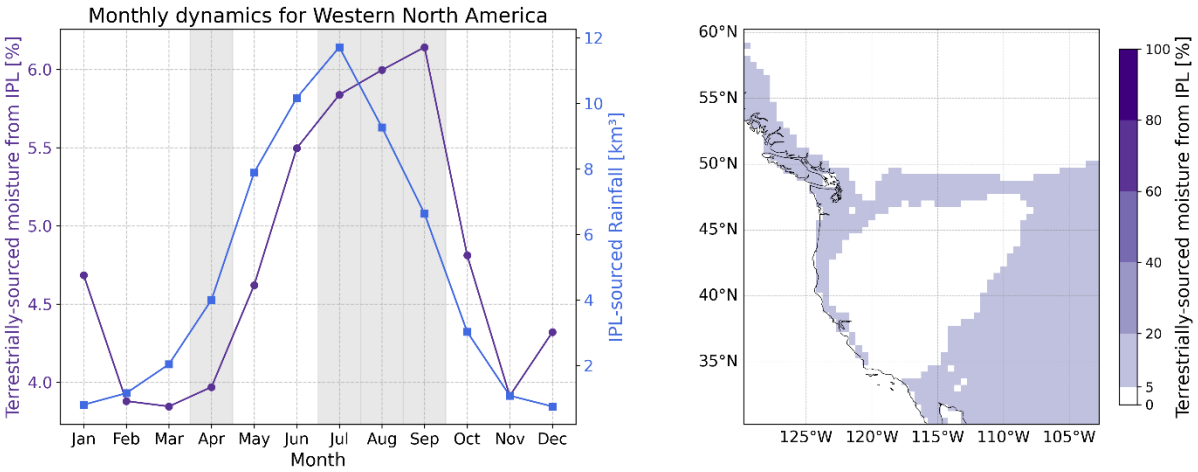

Figure 12: Regional analysis for each Giorgi region (a-u). The left panel shows the IPL sourced moisture per month both in terms of volume (km³, blue line) and percentage of terrestrially sourced moisture (purple line). The dry season is indicated by the months shaded in grey. The right panel displays the proportion of terrestrially-sourced precipitation from IPL for each grid within the cropped Giorgi region.

Taking the Amazon (AMZ) region as an illustrative example: the region as a whole receives 21.4% of its terrestrially-sourced precipitation from IPL (Table 4), this reflects the mean value of all grids in the map view in Figure 12b (AMZ; right panel). Though the region average is 21.4%, there is a hotspot in the north which receives over 60% of its terrestrially-sourced precipitation from IPL. There are clear swaths over the continent from east to west with decreasing dependence on IPL moisture from over 40% down to 0% along parts of the east coast. This gradient can be explained by two factors: 1) In the North Eastern part of Brazil there are only a few sparse and small IPL acting as sources; 2) the main prevailing wind direction is towards the West. Closer to the Andes, the direction of the moisture transport follows the shifts in the ICTZ. Looking at the monthly breakdown of terrestrially sourced moisture from IPL in the Amazon region (left panel), it can be seen that the volume and the proportion follow the same annual cycle. The peak of IPL sourced precipitation is occurring from November – April, with between ~230 – 275 km^3 per month (blue line). This roughly coincides with the months where the IPL proportion of the terrestrially sourced moisture is highest, November – March, with between ~23-25%. The four driest months in the Amazon are June – September, which coincide with the lowest volume (~170 - 205 km^3 per month; blue line) and proportion (18-20%; purple line) of IPL moisture in the region. The seasonality of the flows are influenced by the temporal dynamics of the South American Monsoon System, arising due to complex land-atmosphere interactions at continental scale. The forests in this region provide the necessary latent heat flux (due to moisture condensation) to maintain the monsoon.

Taking the West Africa (WAF) region as an illustrative example: the region as a whole receives 40.21% of its terrestrially-sourced precipitation from IPL (Table 4), this reflects the mean value of all grids in the map view in Figure 12t (WAF; right panel). Though the region average is 40.21%, there is a hotspot in the northwest which receives over 80% of its terrestrially-sourced precipitation from IPL. There are clear swaths over the continent from west to east with decreasing dependence on IPL moisture from over 60% down to under 20%. Looking at the monthly breakdown of terrestrially sourced moisture from IPL in the West Africa region (left panel), it can be seen that the volume and the proportion do not follow the same annual cycle. The peak of IPL sourced precipitation is occurring from July – October, with between ~165 – 220 km^3 per month (blue line). During this time, the IPL proportion of terrestrially sourced moisture is relatively moderate with between ~37-41% (purple line). The highest proportion of terrestrially sourced moisture from IPL coincides with the four driest months, November – February (shaded in grey), with between ~43-46%, when the total volume of IPL moisture input to the region is lowest, ~60 - 110 km^3 per month (blue line).

The examples of the Amazon and West Africa regions represent two difference cases, one where the IPL moisture input to the region peaks in volume and proportion in the same months, and one where the inverse is true, the driest four months are the peak of IPL proportional input to the region. For regions in the case of the latter, the relative importance of IPL moisture increases in the dry season when there is a reduction of ocean sourced moisture, demonstrating an outsized role of IPL for sourcing precipitation in the dry season. This could be explained by IPL which are forested or at least functioning at the ecosystem scale in a way that critical green water flux is still produced in the dry season, and therefore buffering the region in this time. Contributions during the dry season, when water deficits are most acute, are important for maintaining ecological functions and supporting agricultural production.

Figure 8 in section 4.1 shows the 12 monthly global IPL evaporationsheds. We cropped this global data according to the Giorgi regions used in this regional analysis to provide the same monthly analysis at the regional scale and show the seasonality of the regional IPL evaporationsheds. To animate the progression of changes in the spatial extent and precipitation amounts, the monthly evaporationsheds for each region have been compiled into a GIF looping through the months (provided digitally upon request). Here we display the individual months (which make up the GIF) in a small size and for the two illustrative regions, the Amazon and West Africa, for space considerations (Figure 13).

As described in section 4.1 for the global IPL evaporationshed, seasonal changes in atmospheric circulation and temperature result in noticeable differences in the spatial extent and amount of moisture flow throughout the year of the regional IPL evaporationsheds. In the Amazon illustrative example (Figure 13), from November – March the IPL evaporationshed is at its most expansive and delivering up to 140 mm of precipitation per month to some locations. In the West Africa illustrative example (Figure 14), from July – September the IPL evaporationshed is at its most expansive and also delivering up to 140 mm of precipitation per month to some locations.

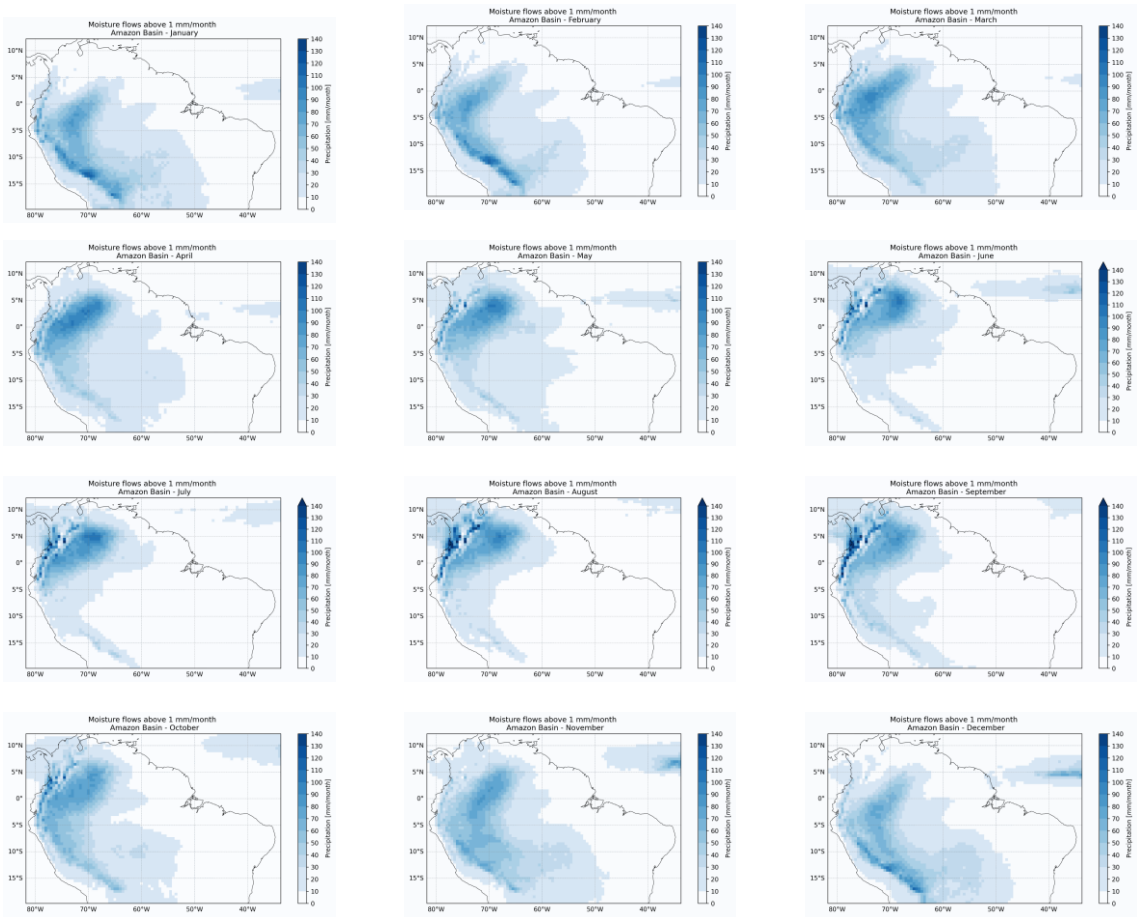

Figure 13: The Amazon (AMZ) regional IPL monthly evaporationshed spatial extents are depicted with amount of precipitation (mm/month) contributed from IPL green water flow (average monthly over the period 2007-2018). Precipitation < 1 mm/month is not displayed. The monthly maps are shown here in a small size for space

considerations; full resolution images are delivered with this report, along with a GIF which loops through these maps to show the monthly progression of the IPL evaporationshed.

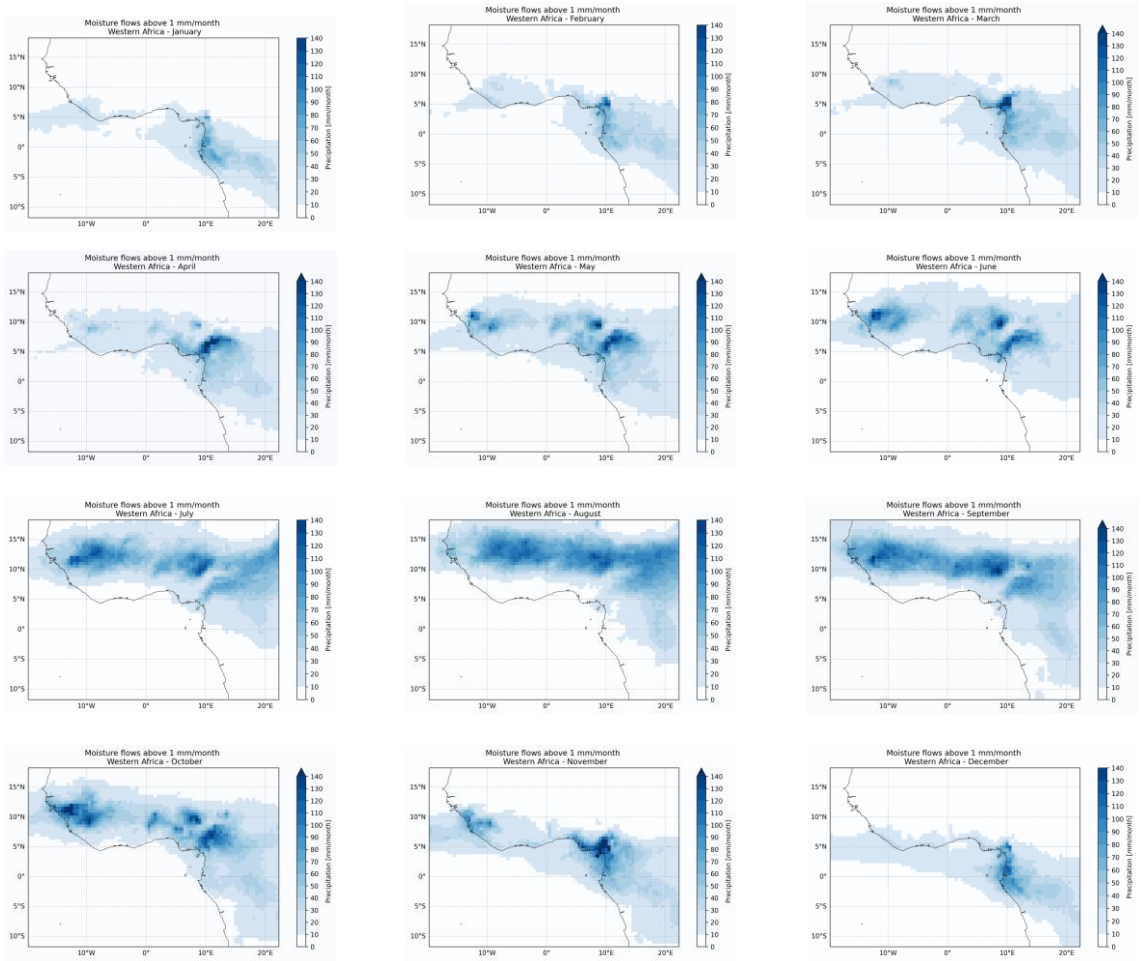

Figure 14: The West Africa (WAF) the regional IPL monthly evaporationshed spatial extents are depicted with amount of precipitation (mm/month) contributed from IPL green water flow (average monthly over the period 2007-2018). Precipitation < 1 mm/month is not displayed. The monthly maps are shown here in a small size for space considerations; full resolution images are delivered with this report, along with a GIF which loops through these maps to show the monthly progression of the IPL evaporationshed.

5. Study Limitations

There are several limitations and sources of uncertainty that must be considered when interpreting the results of this study. The global moisture flow dataset used for this study represents average moisture tracks modeled with UTrack over the period 2007-2018 based on ERA5 climate which we aggregated to the 0.5 deg grid scale. All of the results we surmise are specific to this model set-up and the subsequent post-processing we perform to average results over space and time. The results could be sensitive to:

- Use of a different moisture tracking model
- Use of a different underlying climate dataset to force the moisture tracking model
- Examination of different time periods, for example:
    - an updated current period (i.e. beyond 2018)
    - a longer historical period (i.e. before 2007) to capture the moisture flow network e.g. before specific regions were deforested / converted to agriculture
    - a future time period under different climate change projections- we are aware of one UTrack global dataset which utilizes SSP scenarios as modeled by the Norwegian Earth System model (NorESM2), with the data published in Staal et al., 2024.
- Examination at finer spatial resolution if/when such moisture flow data becomes available
- Aggregation of results to look at different time-scales, e.g. intra-annual variability rather than the period average
- Aggregation of results to look at different spatial scales, e.g. basins or forests rather than regions

The UTrack model has a simplified representation of atmospheric processes, allowing for relatively fast simulation at the global scale. This positive aspect also creates some limitations, though more complexity, different assumptions, and explicit or dynamic process representations would not necessarily improve results, but would certainly change the results. Known model limitations are:

- Precipitation is implicitly represented with a simple moisture accounting scheme, not dynamically simulated through cloud microphysics, which makes it difficult for the model to capture moisture flows which are convective in nature
- Evaporated moisture (in this study, the green water flow or ET) is vertically mixed evenly among the atmospheric layers, not physically resolved according to turbulence
- Long-range vs short-range precipitation source contributions can be distorted by the moisture tracking scheme, where moisture loss is treated as a proportional sink, according to the local (i.e. ERA5 grid value) precipitation fraction of the atmospheric column
- UTrack relies on reanalysis data and will inherit any error present in the underlying atmospheric data
- UTrack is an offline moisture tracking model with no feedbacks between source and sink regions and how they might alter atmospheric circulation or precipitation, this means that land use changes within the simulation period do not influence wind, pressure fields or convection witin the model (they are only represented to the extent they are reflected in the reanalysis data).

- A full description of the UTrack model and its inherent uncertainties can be found in Tuinenburg & Staal, 2020

A major finding of the study was that IPL and non-IPL moisture contributions scale with their proportion of land at the global scale. From this, it could be concluded that IPL and non-IPL perform equally. Future research could aim to disentangle this finding further than we were able to with the regional and dry season analysis, by focusing in on local areas with hotspots of IPL recycling ratios (e.g. > 60% in Figure 9). Regional and sub-regional analysis can be done simply cropping the global dataset to the area of interest, as we have done here with the Giorgi region mask. The only regional dataset we are aware is by Staal et al., 2018b, which is a regional Amazon moisture flow dataset from the UTrack model, with the advantage of a higher grid resolution (0.25 deg) as compared to the global UTrack dataset used here (0.5 deg).

The ET recycling ratios of IPL and non-IPL also performed similarly. The ET recycling ratio of any grid first depends on the amount of green water flow and next on the flow network itself, which determines its fate over land or the ocean. A locations land use / land cover will impact green water flow availability and dynamics, as well as exert some local control on e.g. temperature, surface albedo and winds, which creates feedbacks to the moisture flows themselves. Land stewardship can directly impact these factors and contribute to maintenance, improvement or degradation of an area's ET recycling ratio. However, large-scale circulation patterns and seasonal cycles are exerting a larger control on the global moisture flow network. In this way, if a grid is IPL or non-IPL, and how that land is managed, is of less consequence as its position on in the flow network.

It is also important to consider that ET from land is largely determined by evaporative demand, i.e., physical hydro-climatic processes, which means land-use in some areas might not be the determinant factor on green water flows. It could be that flow from agricultural lands, poorly managed lands and lands lacking in biodiversity have a similar ET rate to an intact forest and land under proper stewardship, based on the evaporative demand alone. Given this, a relevant question going forward could be to understand what is the dominant driver of ET for a certain area: is it evaporative demand (energy-limited) or the availability of green water (water-limited)? When it is the latter, then stewardship and land-use will impact the moisture flows, when it is the former, their influence will be less visible. Particularly in the dry season, when evaporative demand is higher, then the availability of green water will depend on the land cover.

This study looked at regionally-defined dry seasons, which are predicable every year, but future work could also look at drought years and other extreme events specifically. For example, an agricultural area that is irrigated might have ET rates similar to a naturally vegetated area under average conditions, but during an extreme drought period, if agricultural area can't be irrigated to the extent that it usually is, that would cut off green water flow from that landscape, whereas an ecosystem with high biodiversity/functional diversity might still have ET like usual. As we advance further into a world of rising temperatures and more extreme events, which are not captured in our analysis of the period 2007-2018, it is likely that intact and functioning ecosystems will be far better at buffering and sustaining moisture flows.

6. References

Cropper, S., Solander, K., Newman, B. D., Tuinenburg, O. A., Staal, A., Theeuwen, J. J. E., & Xu, C. (2021). Comparing deuterium excess to large-scale precipitation recycling models in the tropics. *Npj Climate and Atmospheric Science*, *4*(1), 60. https://doi.org/10.1038/s41612-021-00217-3

De Petrillo, E., Fahrländer, S. F., Tuninetti, M., Andersen, L. S., Monaco, L., Ridolfi, L., & Laio, F. (2025). Reconciling tracked atmospheric water flows to close the global freshwater cycle. *Communications Earth & Environment*, *6*(1), 347. https://doi.org/10.1038/s43247-025-02289-y

Fa, J. E., Watson, J. E., Leiper, I., Potapov, P., Evans, T. D., Burgess, N. D., Molnár, Z., Fernández-Llamazares, Á., Duncan, T., Wang, S., Austin, B. J., Jonas, H., Robinson, C. J., Malmer, P., Zander, K. K., Jackson, M. V, Ellis, E., Brondizio, E. S., & Garnett, S. T. (2020). Importance of Indigenous Peoples' lands for the conservation of Intact Forest Landscapes. *Frontiers in Ecology and the Environment*, *18*(3), 135–140. https://doi.org/10.1002/fee.2148

Falkenmark, M., & Rockström, J. (1996). Escaping from Ongoing Land/Water Mismanagement. *Ambio*, *25*(3), 211–212.

Fletcher, M.-S., Hamilton, R., Dressler, W., & Palmer, L. (2021). Indigenous knowledge and the shackles of wilderness. *Proceedings of the National Academy of Sciences*, *118*(40). https://doi.org/10.1073/pnas.2022218118

Garnett, S. T., Burgess, N. D., Fa, J. E., Fernández-Llamazares, Á., Molnár, Z., Robinson, C. J., Watson, J. E. M., Zander, K. K., Austin, B., Brondizio, E. S., Collier, N. F., Duncan, T., Ellis, E., Geyle, H., Jackson, M. V., Jonas, H., Malmer, P., McGowan, B., Sivongxay, A., & Leiper, I. (2018). A spatial overview of the global importance of Indigenous lands for conservation. *Nature Sustainability*, *1*(7), 369–374. https://doi.org/10.1038/s41893-018-0100-6

Giorgi, F., & Francisco, R. (2000). Uncertainties in regional climate change prediction: a regional analysis of ensemble simulations with the HADCM2 coupled AOGCM. *Climate Dynamics*, *16*(2–3), 169–182. https://doi.org/10.1007/PL00013733

Hersbach, H., Bell, B., Berrisford, P., Hirahara, S., Horányi, A., Muñoz-Sabater, J., Nicolas, J., Peubey, C., Radu, R., Schepers, D., Simmons, A., Soci, C., Abdalla, S., Abellan, X., Balsamo, G., Bechtold, P., Biavati, G., Bidlot, J., Bonavita, M., … Thépaut, J.-N. (2020). The ERA5 global reanalysis. *Quarterly Journal of the Royal Meteorological Society*, *146*(730), 1999–2049. https://doi.org/https://doi.org/10.1002/qj.3803

Keys, P. (2016). *The Precipitationshed: Concepts, Methods, and Applications*. https://doi.org/10.13140/RG.2.2.20177.84322

Owen, J. R., Kemp, D., Lechner, A. M., Harris, J., Zhang, R., & Lèbre, É. (2022). Energy transition minerals and their intersection with land-connected peoples. *Nature Sustainability*, *6*(2), 203–211. https://doi.org/10.1038/s41893-022-00994-6

Staal, A., Meijer, P., Nyasulu, M. K., Tuinenburg, O. A., & Dekker, S. C. (2024). *Global terrestrial moisture recycling in Shared Socioeconomic Pathways*. https://doi.org/10.5194/egusphere-2024-790

Staal, A., Tuinenburg, O. A., Bosmans, J. H. C., Holmgren, M., van Nes, E. H., Scheffer, M., Zemp, D. C., & Dekker, S. C. (2018a). Forest-rainfall cascades buffer against drought across the Amazon. *Nature Climate Change*, *8*(6), 539–543. https://doi.org/10.1038/s41558-018-0177-y

Staal, A., Tuinenburg, O. A., Bosmans, J. H. C., Holmgren, M., van Nes, E. H., Scheffer, M., Zemp, D. C., & Dekker, S. C. (2018b). Forest-rainfall cascades buffer against drought across the Amazon. *Nature Climate Change*, *8*(6), 539–543. https://doi.org/10.1038/s41558-018-0177-y

Sze, J. S., Childs, D. Z., Carrasco, L. R., & Edwards, D. P. (2022). Indigenous lands in protected areas have high forest integrity across the tropics. *Current Biology*, *32*(22), 4949-4956.e3. https://doi.org/10.1016/j.cub.2022.09.040

Tuinenburg, O. A., & Staal, A. (2020). Tracking the global flows of atmospheric moisture and associated uncertainties. *Hydrology and Earth System Sciences*, *24*(5), 2419–2435. https://doi.org/10.5194/hess-24-2419-2020

van der Ent, R. J., & Savenije, H. H. G. (2013). Oceanic sources of continental precipitation and the correlation with sea surface temperature. *Water Resources Research*, *49*(7), 3993–4004. https://doi.org/10.1002/wrcr.20296

van der Ent, R. J., Savenije, H. H. G., Schaefli, B., & Steele-Dunne, S. C. (2010). Origin and fate of atmospheric moisture over continents. *Water Resources Research*, *46*(9). https://doi.org/https://doi.org/10.1029/2010WR009127

Wunderling, N., Staal, A., Sakschewski, B., Hirota, M., Tuinenburg, O. A., Donges, J. F., Barbosa, H. M. J., & Winkelmann, R. (2022). Recurrent droughts increase risk of cascading tipping events by outpacing adaptive capacities in the Amazon rainforest. *Proceedings of the National Academy of Sciences*, *119*(32). https://doi.org/10.1073/pnas.2120777119